

2mly

FINAL REPORT

N.A.S.A. Grant NGR-47-006-050

PRECISE MEASUREMENT OF CHARGED DEFECTS IN III-V COMPOUNDS (Supplement 2)

November, 1973

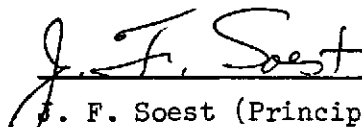
(NASA-CR-138076) PRECISE MEASUREMENT OF  
CHARGED DEFECTS IN III-V COMPOUNDS  
(SUPPLEMENT 2) Final Report (College of  
William and Mary) 95 p HC \$7.75

N74-21359

Unclass  
16010

CSCL 20L G3/26

Report prepared by

  
J. F. Soest (Principal Investigator)

Participants in this Research

Richard K. Hester

Arden Sher

Jon F. Soest

Gideon Weisz

With special gratitude for the assistance of

LeRoy H. Botten

Kent Cueman

Patricia Millington

Michael Schmidt

## Table of Contents

	Page No.
I. INTRODUCTION. . . . .	1
II. THEORETICAL ANALYSIS OF NUCLEAR RESONANCE LINE SHAPES . . . . .	3
III. EXPERIMENTAL EQUIPMENT. . . . .	13
IV. ANALYSIS OF DATA. . . . .	19
FOOTNOTES . . . . .	31
Appendix A    Article submitted to Review of Scientific Instruments . . . . .	33
Appendix B    Articles in preparation. . . . .	33

## I. INTRODUCTION

In the past few years, improvements in the growth of epitaxial and bulk crystal forms of III-V compound semiconductor materials have led to many new devices. These devices include Gunn oscillators, light emitting diodes, infrared detectors, lasers, and special purpose transistors. The performance and lifetime of such devices depends sensitively on defects in the material. For example, the intensity of light emitting diodes is known to be strongly affected by dislocations that can be initiated by point defects.

Most impurities in III-V compounds can be detected in very low concentrations by chemical means. Vacancies, however, are difficult to detect. For this reason unexplained phenomena observed in these materials are often blamed on vacancies. It has been claimed that vacancies act as traps, recombination centers, and scattering centers. Since no method has existed to directly detect the vacancies, it has been difficult to confirm such assertions. Once low concentrations of vacancies can be detected, then their supposed effects can be confirmed; and, what is more important, crystal growth methods can be improved to eliminate them.

The purpose of this work has been to develop experimental methods and related theory which will permit the measurement of low concentrations of vacancies and other defects in III-V compound semiconductors. Once the nature of these defects has been determined, this information can be incorporated into a transport theory for devices constructed from these materials, and experiments

conducted to test the theory.

The vacancies and other defects in the III-V compounds are detected by measurement of the nuclear magnetic resonance (NMR) line width. Most of the III-V compounds have at least one isotope with a nuclear quadrupole moment. In a crystal with a cubic crystal field (characteristic of most III-V compounds) there is no quadrupole splitting of the Zeeman resonance line. However, a defect removes the cubic symmetry locally and causes splittings which result in a change of the NMR line width. This change can be used to detect the presence of vacancies in concentrations as low as  $10^{14}/\text{cm}^3$ .<sup>1</sup>

This report describes the progress to date on the project, as supported by this research grant. Further reports will be made in the form of publications that are now being prepared for submission to scientific journals. Copies of these will be forwarded to NASA as they are completed. One of these reports has been submitted to the Review of Scientific Instruments for publication, and is included as Appendix A to this report.

## II. THEORETICAL ANALYSIS OF NUCLEAR RESONANCE LINE SHAPES

The objective of this section is to compute the nuclear magnetic resonance (NMR) line broadening for the spins in a III-V compound semiconductor, in the large magnetic field limit. The spins interact normally via dipole-dipole and exchange interactions. In addition, charged point defects, such as vacancies or ionized donors and acceptors, break the cubic crystal symmetry and create a distribution of electric field gradients - and so quadrupole shifts - in their neighborhood. The electric field due to these charged defects shifts the ions around them from their equilibrium lattice sites into regions with finite electric field gradients. Such off-lattice site field gradients are large compared to those arising directly from the point charges. Since the electric field decreases only as the square of the distance  $r$  from each defect, each defect influences many ions.

For low concentrations of defects where most ions experience small fields, the quadrupole shifts broaden the Zeeman lines. If the fields decrease as  $r^{-2}$  the line shapes are Gaussian; if the fields arise from something like a dipolar charge distribution and fall off as fast as  $r^{-3}$  the line shapes are Lorentzian. However, when the concentrations are higher, the shifts become large enough so that only the transitions between the levels identified by  $z$ -components of spin  $+1/2$  and  $-1/2$  remain in the original Zeeman line, and the intensity is

reduced. The width of this remaining line decreases because with these large quadrupole splittings some parts of the dipole-dipole and exchange interactions become non-secular. An experimental study of these effects will provide information about defect concentrations, and possibly the charge distributions about defects.

### Spin Hamiltonian

The Hamiltonian for the system is:

$$\mathcal{H} = \mathcal{H}_Z + \mathcal{H}_{dd}^s + \mathcal{H}_{ex} + \mathcal{H}_Q. \quad (1)$$

The Zeeman Hamiltonian is:

$$\mathcal{H}_Z = -\sum_l \gamma_l \vec{I}_l \cdot \vec{H}, \quad \vec{H} = H \hat{n}, \quad (2)$$

where nucleus  $l$  has gyromagnetic ratio  $\gamma_l$  and spin  $\vec{I}_l$ .

For like spins, and when  $\mathcal{H}_Q = 0$ , the secular part of the dipole-dipole plus pseudo dipole-dipole Hamiltonian is:

$$\mathcal{H}_{dd}^s = \sum_{l,l'}' \left( \frac{\gamma_l \gamma_{l'}}{4 r_{ll'}^3} + B_{ll'} \right) (3 \cos^2 \theta_{ll'} - 1) (\vec{I}_l \cdot \vec{I}_{l'} - 3 \vec{I}_l \cdot \hat{n} \hat{n} \cdot \vec{I}_{l'}). \quad (3)$$

Where the pseudo dipolar coupling constant  $B_{ll'}$  arises from indirect interactions between the  $l$  and  $l'$  nuclei coupled by p and d electrons. For unlike spins, a part of  $\vec{I}_l \cdot \vec{I}_{l'}$  does not contribute to the secular Hamiltonian. The changes when  $\mathcal{H}_Q \neq 0$  will be discussed in detail later.

The exchange Hamiltonian is:

$$\mathcal{H}_{ex} = \sum_{l,l'}' A_{ll'} \vec{I}_l \cdot \vec{I}_{l'}, \quad (4)$$

where  $A_{ll'}$  is the exchange coupling constant that arises from interactions among the nuclei and s electrons.<sup>2</sup>  $A_{ll'}$  is independent of the direction of the magnetic field, and thus produces isotropic changes in the line shape.

The secular part of the quadrupole Hamiltonian is:

$$\mathcal{H}_Q^s = \sum_l \frac{e^2 Q_l}{4I_l(2I_l-1)} \hat{n} \cdot \underset{\sim}{q}_l^l \cdot \hat{n} [3(\vec{I}_l \cdot \hat{n})^2 - I_l(I_l+1)] \quad (5)$$

where  $Q_l$  is the quadrupole moment of nucleus  $l$ , and the field gradient tensor  $\underset{\sim}{q}_l^l$  is produced by the electric field  $\vec{E}^l$  at site  $l$ ,

$$eq_{fij}^l = \sum_k R_{ijk}^l E_k^l \quad (6)$$

The indices  $i, j, k = x, y, z$  run over the principal cubic axes of the crystal.

The piezoelectric strain terms and the direct field gradient terms have been dropped from  $eq_{fij}^l$  because they are small compared to the field generated terms. The III-V compounds all have a  $T_d$  symmetry for which

$$\underset{\sim}{eq}_f^l = -R^l \begin{pmatrix} 0 & E_z^l & E_y^l \\ E_z^l & 0 & E_x^l \\ E_y^l & E_x^l & 0 \end{pmatrix} \quad (7)$$

where  $R^l$  is the value of the only non-vanishing elements of the  $\underset{\sim}{R}^l$  tensor at site  $l$ ,  $R^l \equiv R_{xyz}^l = R_{yzx}^l = R_{zxy}^l$ . In the III-V compounds,  $R^l$  takes on only two values, one for III-atom sites, and the other for V-atom sites.

Finally, from Eq. (6) we find:

$$\hat{n} \cdot \underset{\sim}{eq}_f^l \cdot \hat{n} = -2R^l (n_x n_y E_z^l + n_x n_z E_y^l + n_y n_z E_x^l) \quad (8)$$

Since most of the nuclei affected by an impurity lie outside the first few near neighbor shells, a reasonably accurate approximation for the electric field at displacement  $\vec{r}$  from an impurity is:

$$\vec{E} = \frac{e^* \vec{r}}{\epsilon r^3} \quad (9)$$



where  $e^*$  is the effective charge of the impurity and  $\epsilon$  is the low frequency dielectric constant. Justification for such a simple form for the electric field in an insulator is given by Kubo.<sup>3</sup> If, as we hope, experiments can be devised that provide detailed information about the charge distribution near an impurity, then a more accurate dielectric response formulation will be needed. However, useful insights can be gained from an analysis of this simple model.

Since the initial experiments have been conducted on GaAs, the remainder of this discussion will be specialized to the spin 3/2 case (the spin of  $\text{Ga}^{69}$ ,  $\text{Ga}^{71}$ , and  $\text{As}^{75}$ ). The experimentally determined values<sup>4</sup> of  $R^{\text{Ga}} = 0.98 \times 10^{10} \text{ cm}^{-1}$  and  $R^{\text{As}} = 1.55 \times 10^{10} \text{ cm}^{-1}$  will be used. The natural abundances, gyromagnetic ratios, and quadrupole moments for the nuclei in GaAs are given in Table I.

Nucleus	Natural Abundance (per cent)	Gyromagnetic Ratio (kHz per gauss)	Quadrupole Moment ( $\text{cm}^2$ )
$\text{Ga}^{69}$	60.2	1.0219	$.178 \times 10^{-24}$
$\text{Ga}^{71}$	39.8	1.2984	$.112 \times 10^{-24}$
$\text{As}^{75}$	100	0.7292	$.3 \times 10^{-24}$

Table I.

#### Calculation of the Number of Spins Influenced by a Defect

Let us concentrate on one of the isotopes with Larmor frequency denoted by  $\nu = \gamma H$ . The magnitude of the shift of the Larmor frequency  $\Delta\nu$  of the

$m \equiv I_z$  transitions from the states  $3/2$  to  $1/2$  and  $-3/2$  to  $-1/2$  of an ion at displacement  $\vec{r}$  relative to an impurity is

$$\Delta V = \frac{eQe^*q_{zz}3\Delta(m^2)}{4I(2I-1)h} = -\vec{\alpha} \cdot \frac{\vec{r}}{r^3} \quad (10)$$

where

$$\vec{\alpha} \equiv \frac{eQe^*R}{\epsilon h} (n_x n_y \hat{z} + n_x n_z \hat{y} + n_y n_z \hat{x}) \quad (11)$$

In order to compare our experiments with Rhoderick's<sup>5</sup> experiments on the variation of NMR intensity with ionized impurity concentrations, or to compute the change of the line shape, the number of ions near an impurity whose quadrupole frequency shift  $|\Delta v|$  is greater than some prescribed minimum  $\Delta v_{\min}$  must be found. To accomplish this we shall first calculate the volume near a given impurity where  $|\Delta v| > \Delta v_{\min}$ . In order to take account of finite size effects and avoid infinities that arise from the fact that  $r^{-2}$  falls off slowly, we shall actually compute the volume  $\Omega$  of the sample for which  $|\Delta v| > \Delta v_{\min}$ , and also  $r < r_0$ , where  $r_0$  will be a characteristic dimension of the sample. There will be two cases to treat. In the first instance  $\Delta v$  is small enough so the volume  $\Omega$  is limited by  $r_0$ , and in the second case  $\Delta v$  is sufficiently large so the volume  $\Omega$  lies completely within the sample.

This model for the finite size is a bit too simple, since it is correct only for an impurity located at the center of a spherical sample. A more accurate model would round off some of the abrupt changes this simple model introduces. We will find, however, that no observable physical phenomena are sensitive to this choice, so it is useless to deal with the complexities

of a more realistic model. The only purpose served by the finite size is to provide a cutoff to eliminate an unphysical infinity.

Another restriction must be placed on the lower limit of  $r$ ,  $a < r$ , to account for the fact that the host atoms are separated from the impurity by at least a distance  $a$ . For example, if the resonant nucleus is a type III nucleus, and the vacancy or impurity is at a type V site, then  $a$  is the near neighbor distance  $a_0$ . If the defect sits on a type III site, then  $a$  is larger ( $a = (8/3)^{1/2} a_0$ ). If the defect is in an interstitial site, then  $a$  will be less than  $a_0$ .

From Eq. (10), the condition that  $\Delta v$  be constant is satisfied for

$$r^2 = -\frac{\Delta v}{\alpha} \cos \theta \quad (12)$$

where  $\theta$  is the angle between  $\hat{r}$  and  $\hat{\alpha}$ . The broadening of the magnetic resonance lines and the decrease in intensity depends only on the magnitude of  $\Delta v$ ; positive and negative values contribute equally. Thus the shape of the volume with  $|\Delta v| > \Delta v_{\min}$  and  $a < r < r_0$  is a figure of revolution about the direction  $\vec{\alpha}$ , of the shaded area shown in Figure 1.

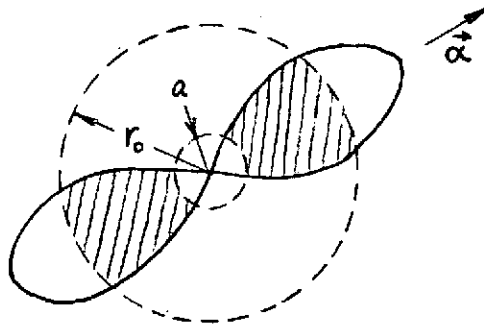


Fig. 1

For this case, the volume  $\Omega$  is given by the integral

$$\begin{aligned}\Omega(\Delta\nu) &= 4\pi \int_0^{\cos^{-1}(r_0^2 \Delta\nu/\alpha)} \sin\theta d\theta \int_0^{r_0} r^2 dr + 4\pi \int_{\cos^{-1}(r_0^2 \Delta\nu/\alpha)}^{\pi/2} \sin\theta d\theta \int_0^{\sqrt{\alpha \cos\theta/\Delta\nu}} r^2 dr - \\ &\quad - 4\pi \int_0^{\cos^{-1}(a^2 \Delta\nu/\alpha)} \sin\theta d\theta \int_0^a r^2 dr - 4\pi \int_{\cos^{-1}(a^2 \Delta\nu/\alpha)}^{\pi/2} \sin\theta d\theta \int_0^{\sqrt{\alpha \cos\theta/\Delta\nu}} r^2 dr \\ &= \frac{4\pi}{3} r_0^3 \left(1 - \frac{3}{5} \frac{r_0^2 \Delta\nu}{\alpha}\right) - \frac{4\pi}{3} a^3 \left(1 - \frac{3}{5} \frac{a^2 \Delta\nu}{\alpha}\right).\end{aligned}\quad (13)$$

Next suppose that  $\Delta\nu$  is large enough so that the volume lies within the sample. Then the volume over which the integral must be taken is a figure of revolution of the solid curve, for  $r > a$ , in Figure 1. Then the integral is:

$$\begin{aligned}\Omega(\Delta\nu) &= 4\pi \int_0^{\pi/2} \sin\theta d\theta \int_0^{\sqrt{\alpha \cos\theta/\Delta\nu}} r^2 dr - \frac{4\pi}{3} a^3 \left(1 - \frac{3}{5} \frac{a^2 \Delta\nu}{\alpha}\right) \\ &= \frac{8\pi}{15} \left(\frac{\alpha}{\Delta\nu}\right)^{3/2} - \frac{4\pi}{3} a^3 \left(1 - \frac{3}{5} \frac{a^2 \Delta\nu}{\alpha}\right).\end{aligned}\quad (14)$$

If  $\rho$  is the density of nuclei of interest, e.g.  $\text{Ga}^{69}$ , then the number  $N_s(\Delta\nu)$  with frequency shift greater than  $\Delta\nu$  is

$$\begin{aligned}N_s(\Delta\nu) &= \rho \Omega(\Delta\nu) \\ &= \begin{cases} N \left[ \left(1 - \frac{3}{5} \frac{\Delta\nu}{\Delta\nu_0}\right) - \frac{a^3}{r_0^3} \left(1 - \frac{3}{5} \frac{\Delta\nu}{\Delta\nu_m}\right) \right], & \Delta\nu < \Delta\nu_0 \\ N \left[ \frac{2}{5} \left(\frac{\Delta\nu_0}{\Delta\nu}\right)^{3/2} - \frac{a^3}{r_0^3} \left(1 - \frac{3}{5} \frac{\Delta\nu}{\Delta\nu_m}\right) \right], & \Delta\nu_0 < \Delta\nu < \Delta\nu_m \\ 0, & \Delta\nu > \Delta\nu_m \end{cases}\end{aligned}\quad (15)$$

where

$$\begin{aligned}\Delta\nu_0 &\equiv \alpha/r_0^2 = \frac{eQe^*R}{\epsilon h r_0^2} \sqrt{(n_x n_y)^2 + (n_x n_z)^2 + (n_y n_z)^2}, \\ \Delta\nu_m &\equiv \alpha/a^2,\end{aligned}\quad (16)$$

and  $N$  is the number of relevant ions ( $\text{Ga}^{69}$ ) in the sample.

### Calculation of the Line Shape Due to the Defect-Induced Quadrupole Interaction

The distribution  $g(\Delta\nu)$  of frequency shifts between  $\Delta\nu$  and  $\Delta\nu + d(\Delta\nu)$  caused by a single impurity is related to  $N_g(\Delta\nu)$  by the expression

$$g(\Delta\nu) = -\frac{dN_g(\Delta\nu)}{d\Delta\nu} = \frac{3}{5} \frac{N}{\Delta\nu_0} \begin{cases} 1 - (\Delta\nu_0/\Delta\nu_m)^{5/2}, & \Delta\nu < \Delta\nu_0 \\ (\Delta\nu_0/\Delta\nu)^{5/2} - (\Delta\nu_0/\Delta\nu_m)^{5/2}, & \Delta\nu_0 < \Delta\nu < \Delta\nu_m \\ 0, & \Delta\nu > \Delta\nu_m \end{cases} \quad (17)$$

Thus  $g(\Delta\nu)$  is constant until  $\Delta\nu$  reaches  $\Delta\nu_0$ , then decreases as  $(\Delta\nu)^{-5/2}$  until  $\Delta\nu$  reaches its maximum value  $(r_0^2/a^2)\Delta\nu_0 = (\alpha/a^2)$ , where  $g(\Delta\nu)$  goes to zero.

Next we must find the line shape and width to associate with a number of impurities distributed at random throughout the sample. For a broadening mechanism caused by dilute impurities, it is well known<sup>6</sup> that if the interaction between the impurity and the major constituent nuclei falls off faster than  $r^{-2}$  then the line shape is Lorentzian. However, if the interaction falls off as  $r^{-2}$  or slower, then the conditions for the "Central Limits Theorem" are satisfied and the line shape is Gaussian. Since the model we are investigating has the fields decreasing as  $r^{-2}$ , we shall use the results of the Central Limits Theorem.

The second moment of the Gaussian  $\overline{\Delta\nu^2}$ , according to the Central Limits Theorem, equals the second moment  $\overline{\Delta\nu_1^2}$  of the one impurity distribution times the number of impurities  $N_I$ .

$$\begin{aligned} \overline{\Delta\nu^2} &= N_I \overline{\Delta\nu_1^2} = N_I \frac{\int_0^{\Delta\nu_m} g(\Delta\nu) (\Delta\nu)^2 d\Delta\nu}{\int_0^{\Delta\nu_m} g(\Delta\nu) d\Delta\nu} \\ &= N_I \frac{(\Delta\nu_0)^{3/2} (\Delta\nu_m)^{1/2} [1 - (\Delta\nu_0/\Delta\nu_m)^{1/2}]}{1 - (\Delta\nu_0/\Delta\nu_m)^{3/2}} \end{aligned} \quad (18)$$

$$\approx \frac{4\pi}{3} \rho_I \frac{e^2 Q^2 e^{*2} R^2}{a h^2 \epsilon^2} [(n_x n_y)^2 + (n_x n_z)^2 + (n_y n_z)^2]$$

where  $\rho_I$  is the density of defects.<sup>7</sup> As we stated earlier,  $\overline{\Delta v^2}$  does not depend on the size of the sample,  $r_0$ .

Finally, the relation between the distribution of quadrupole frequency shifts  $G_Q(\Delta v)$  (basically an inhomogeneous broadening), and the NMR line shape  $G(v)$  must be established. The quadrupole frequency shift distribution is a Gaussian function with variance  $\overline{\Delta v^2}$ :

$$G_Q(\Delta v) = \frac{1}{(2\pi \overline{\Delta v^2})^{1/2}} e^{-\Delta v^2 / 2 \overline{\Delta v^2}} \quad (19)$$

For the spin 3/2 case, the magnetic resonance line shape is found through the expression

$$G(v) = \int_{-\infty}^{\infty} d\Delta v G_Q(\Delta v) \left[ .3 G_{1/2, 3/2}(v - \Delta v, \Delta v) + .4 G_{-1/2, 1/2}(v, \Delta v) + .3 G_{-3/2, -1/2}(v + \Delta v, \Delta v) \right], \quad (20)$$

where  $G_{1/2, 3/2}(v - \Delta v, \Delta v)$  is the line shape function of the  $3/2 \rightarrow 1/2$  transition caused by other broadening mechanisms (as modified by the quadrupole shifts). The first argument in the functional dependence of  $G_{1/2, 3/2}$  is the center frequency, and the second is intended to represent the effect the shift may cause on the line shape. The shape due to other interactions can be modified by the shifts, e.g. terms in the dipolar Hamiltonian that are secular in the absence of shifts will become non-secular when the shifts are large enough, thus modifying the width of the dipolar broadened line.  $G_{-1/2, 1/2}$  and  $G_{-3/2, -1/2}$  are the corresponding shape functions for those transitions. The factors 0.3, 0.4, 0.3 multiplying the shape functions are weighting factors which arise from the transition matrix elements for the three transitions.

We shall have to treat the more complex case later, but for now examine the simple situation corresponding to low defect concentrations.

$$G_{\frac{1}{2}, \frac{3}{2}}(\nu - \Delta\nu, \Delta\nu) \approx G_{\frac{1}{2}, \frac{3}{2}}(\nu - \Delta\nu, 0)$$

$$G_{-\frac{1}{2}, \frac{1}{2}}(\nu, \Delta\nu) \approx G_{-\frac{1}{2}, \frac{1}{2}}(\nu, 0)$$

$$G_{-\frac{3}{2}, -\frac{1}{2}}(\nu + \Delta\nu, \Delta\nu) \approx G_{-\frac{3}{2}, -\frac{1}{2}}(\nu, 0)$$

(21)

$$G_{\frac{1}{2}, \frac{3}{2}}(\nu, 0) = G_{-\frac{1}{2}, \frac{1}{2}}(\nu, 0) = G_{-\frac{3}{2}, -\frac{1}{2}}(\nu, 0) = G_0(\nu).$$

Then Eq. (20), in view of the approximation in Eq. (21), becomes

$$G(\nu) = 0.4 G_0(\nu) + 0.6 \int_{-\infty}^{\infty} d\Delta\nu G_0(\nu + \Delta\nu) G_Q(\Delta\nu). \quad (22)$$

If  $G_0(\nu)$  is a Gaussian with variance  $\sigma_0$ , then

$$G(\nu) = \frac{0.6}{\sqrt{2\pi} (\sigma_0^2 + \overline{\Delta\nu^2})^{1/2}} e^{-\frac{\nu^2}{2(\sigma_0^2 + \overline{\Delta\nu^2})}} + \frac{0.4}{\sqrt{2\pi} \sigma_0} e^{-\frac{\nu^2}{2\sigma_0^2}}, \quad (23)$$

where  $\nu$  is centered at the Larmor frequency. Thus the variance  $\sigma_c$  of the composite line is

$$\sigma_c^2 = (\sigma_0^2 + 0.6 \overline{\Delta\nu^2})^{1/2}. \quad (24)$$

The contribution from the quadrupole interaction can also be found from a standard Van Vleck calculation that yields an answer involving a lattice sum.<sup>2</sup> If one uses the electric field-induced gradients, as given in Eq. (16), the angular dependence of  $\sigma_c^2$  is reproduced exactly. If, in addition, the radial lattice sum is replaced with an integral, the same numerical result, Eq. (24), is obtained.

### III. EXPERIMENTAL EQUIPMENT

#### 1. Pulsed NMR

The descriptions of equipment in this section may be clarified by reference to Figure 2, a block diagram of the pulsed NMR system. Much of this system was purchased with funds provided by a National Science Foundation Departmental Development Grant. However, graduate student support and faculty summer salaries provided by this grant were indispensable to the construction of the system.

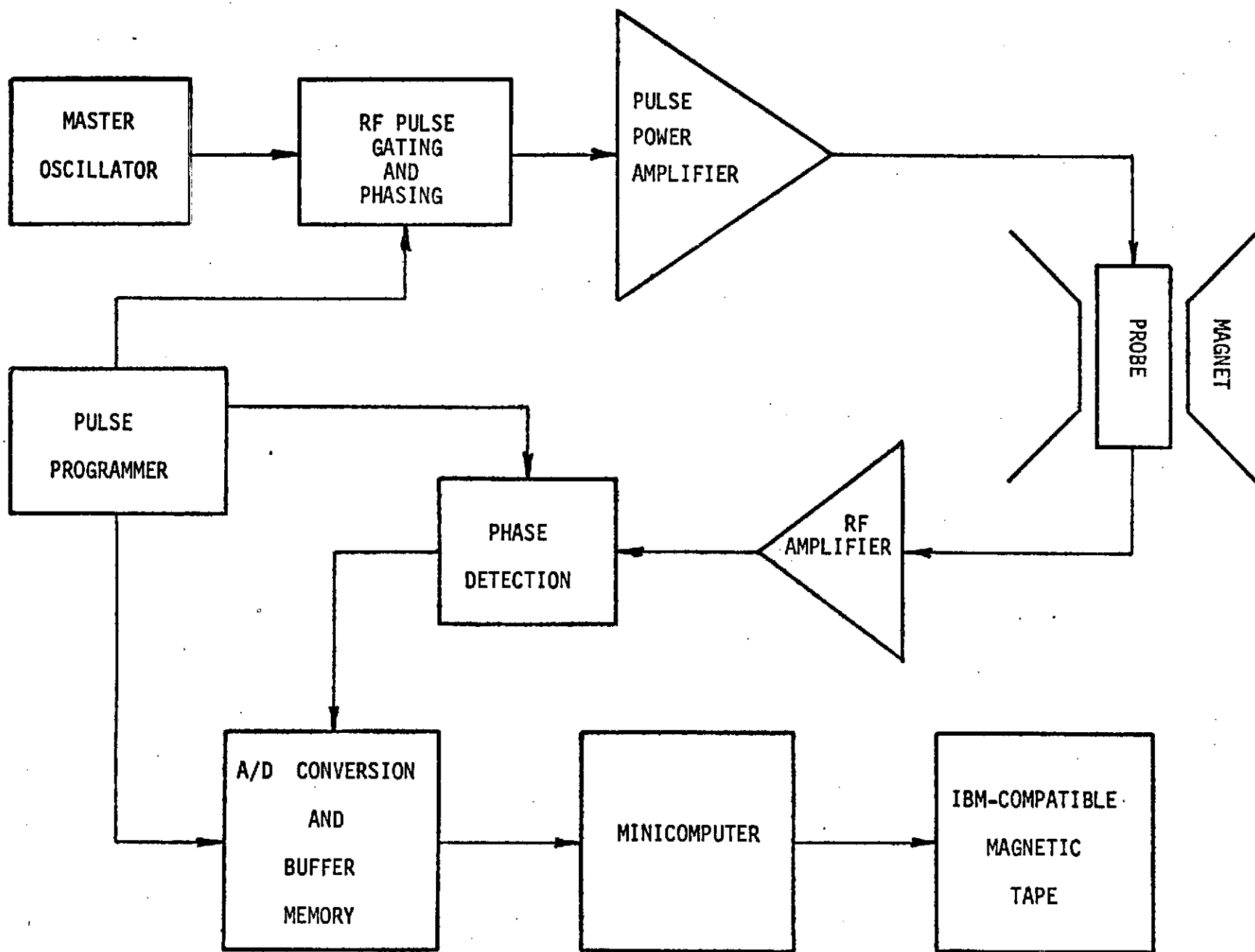
##### a. Pulse programmer

A programmable pulse generator was designed and built in this laboratory to control the sequences of pulses of radio frequency (rf) magnetic field that are applied to the sample. A number of pulses and delays can be called for serially in time. Each pulse can have one of four different rf phases in the gating and phasing circuits. The rf can be supplied either as normal high intensity pulses, or as low and variable intensity pulses for "rotating frame" experiments. Both the pulse duration and the delay time can be controlled either digitally or by analog circuits.

Although the pulse programmer is limited to 16 separate instructions, two capabilities extend its effective memory. Many pulse sequences are repetitions of a basic short sequence. The programmer has two separate counters that permit "looping" of a particular sequence a number of times. In addition, the



Figure 2. Block Diagram of Pulsed NMR Apparatus



pulse programmer memory can be loaded by the minicomputer that controls the signal averaging process. Thus the programmer memory is effectively extended to the memory available in the minicomputer, if there is enough time (approximately 50 microseconds) in a given sequence to reload between pulses.

A more complete description of the programmer is being prepared for publication (see Appendix B).

b. RF Phasing and Gating

This portion of the pulsed NMR system provides pulses of rf in the sequence specified by the pulse programmer. The rf source is a General Radio frequency synthesizer with excellent frequency, amplitude, and phase stability. The pulses may have any one of four phases with respect to the master oscillator:  $0^\circ$ ,  $90^\circ$ ,  $180^\circ$ ,  $270^\circ$ .

Actual pulse gating and amplification are done at a fixed frequency, and the result is mixed with a variable frequency to provide the NMR stimulating pulse. This procedure eliminates much of the tuning usually required to change NMR frequencies.

c. Power Amplifier and Sample Probe

A combination of commercial power amplifiers and circuits made in this laboratory is used to apply the rf pulses to the sample. The main power amplifier is a NMR Specialties P-103R, capable of applying up to five kilowatt rf pulses.

The "single coil" probes that are used combine suggestions by Waugh<sup>8</sup> and Lowe<sup>9</sup>. The rf magnetic fields produced are about 75 gauss, which makes the time for a " $\pi/2$  pulse" for  $\text{Ga}^{69}$  about 3.3 microseconds. Recovery time of the system after a pulse (until the NMR signal may be seen) is on the order of 3 to 5 micro-

seconds at 20 megahertz. For  $\text{Ga}^{69}$  in GaAs, the NMR signal decay time ( $T_2$ ) is about 150 microseconds. Thus our pulse amplitude and recovery time have been more than adequate for these experiments.

#### d. NMR Signal Detection and Averaging

The transient response of the nuclear magnetization after the stimulating rf pulse is amplified and detected by a combination of commercial apparatus, and circuits like those described by Waugh<sup>8</sup> and Lowe.<sup>9</sup> The signal may then be viewed on an oscilloscope screen or undergo analog-to-digital conversion. It is this latter process that provides the large signal-to-noise ratio required for our experiment.

We have constructed a digital processor and computer interface to provide the following signal averaging process: (1) analog-to-digital conversion, (2) temporary storage of data in a high speed buffer memory, (3) transfer of data to the memory of a small computer, (4) averaging and simple manipulation of data by the computer, and (5) transfer of data to IBM-compatible magnetic tape for use on a large scale computer.

The analog-to-digital converter samples the NMR signal at a maximum rate of once every 200 nanoseconds, and converts the amplitude to an eight-bit binary result. This result must be temporarily stored, since the data rate is too high for present-day computers. Timing and data transfer are accomplished with digital circuitry designed and constructed entirely in this laboratory. This circuitry will be described in detail in a paper now in preparation (see Appendix B).

The small computer is a Digital Equipment Corporation PDP-8/E. It has internal interfacing to allow display of memory contents on an oscilloscope, and to record data on a cartridge-style magnetic tape recorder. Simple addition of incoming data to the previous data stored in the computer improves the signal-to-noise ratio, since the signal amplitude adds up more rapidly than the noise.

Memory locations currently available in our computer allow us to sample up to  $1024$  points per transient signal. This provides a very detailed picture of the NMR signal. This signal can be Fourier transformed to show the usual frequency domain line shape, or manipulated directly to find certain average values, such as the second moment.

Another feature available in our interface allows analog-to-digital conversion to be done at selected times during the decay. This aids in analyzing the complicated structure of the signal resulting from a pulse sequence.

Finally, we have constructed a simple interface that permits us to use an IBM-compatible magnetic tape deck for recording the data from our computer. We are then able to transfer the data to the William and Mary IBM 360/Model 50 computer, and to take advantage of the library facilities and peripheral equipment of a full scale computer center. This allows, for example, display of the data by a CalComp plotter-see Figures 3 and 4. A more complete description of the interface has been given in a paper submitted to the Review of Scientific Instruments (Appendix A).

## 2. CW NMR

We have available an NMR spectrometer built by D. R. Torgeson,<sup>10</sup> and a Varian V-4230B crossed-coil rf probe. This combination has an excellent signal-to-noise ratio, and samples and frequencies are easily changed. We also have a

Northern Scientific model NS-561 Signal Averager. This unit has also been interfaced to the small computer, and thus may have its data transferred to the IBM system.

### 3. Magnet

Fields of up to 19.4 kilogauss are provided by a Varian model V-3900 electromagnet and power supply. The field is stabilized with a Varian Mark I Fieldial Hall effect device. This system was chosen for its combination of strength, homogeneity, and stability of field, all of which are essential to the experiments proposed here.

#### IV. ANALYSIS OF DATA

In this section, the results of  $\text{Ga}^{69}$  NMR studies on two different samples of GaAs will be discussed. This represents the data that had been analyzed by the completion date of this grant; however, far more data have been taken and analyzed during this past summer. Those data will be briefly described at the conclusion of this section.

Figures 3 and 4 are computer plots of typical transient NMR signals from the two samples. This signal, usually called the free induction decay (FID), is actually composed of  $1024$  separate data points that have been accumulated by the signal averaging system discussed in Section III. The plotter has interpolated between points, making the signal appear continuous.

A pure, undamaged sample of GaAs gives the  $\text{Ga}^{69}$  FID shown in Figure 3. The signal averaging process is actually initiated before the rf pulse, giving rise to the horizontal baseline to the left of  $t=0$ . At  $t=0$ , the rf pulse is applied, and the FID begins after the pulse. There is a short dead time (about  $10 \mu\text{sec.}$ ), and some noise generated by the piezoelectric response of the crystal at the very beginning of the FID. The remainder of the signal is nearly Gaussian in shape, but with a pronounced oscillation - seen most clearly in the negative-going curve around  $t=480 \mu\text{sec.}$

Figure 4 is the FID of  $\text{Ga}^{69}$  in a GaAs sample that was heated to  $800^\circ\text{C}$  to create vacancies, then quenched rapidly to room temperature to trap them. According to Pearson, Potts, and Macres,<sup>11</sup> the number of vacancies present should

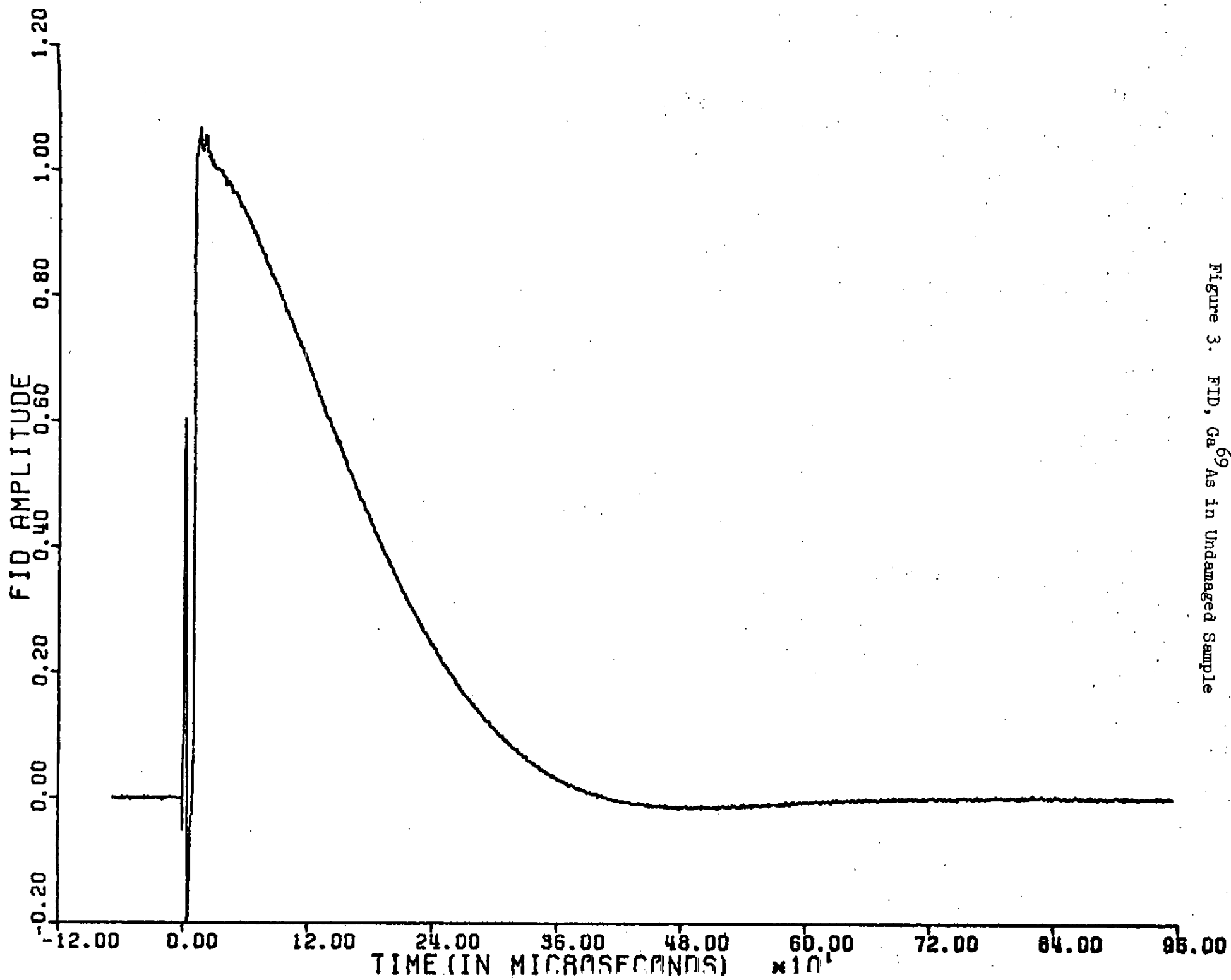


Figure 3. FID, Ga<sup>69</sup>As in Undamaged Sample

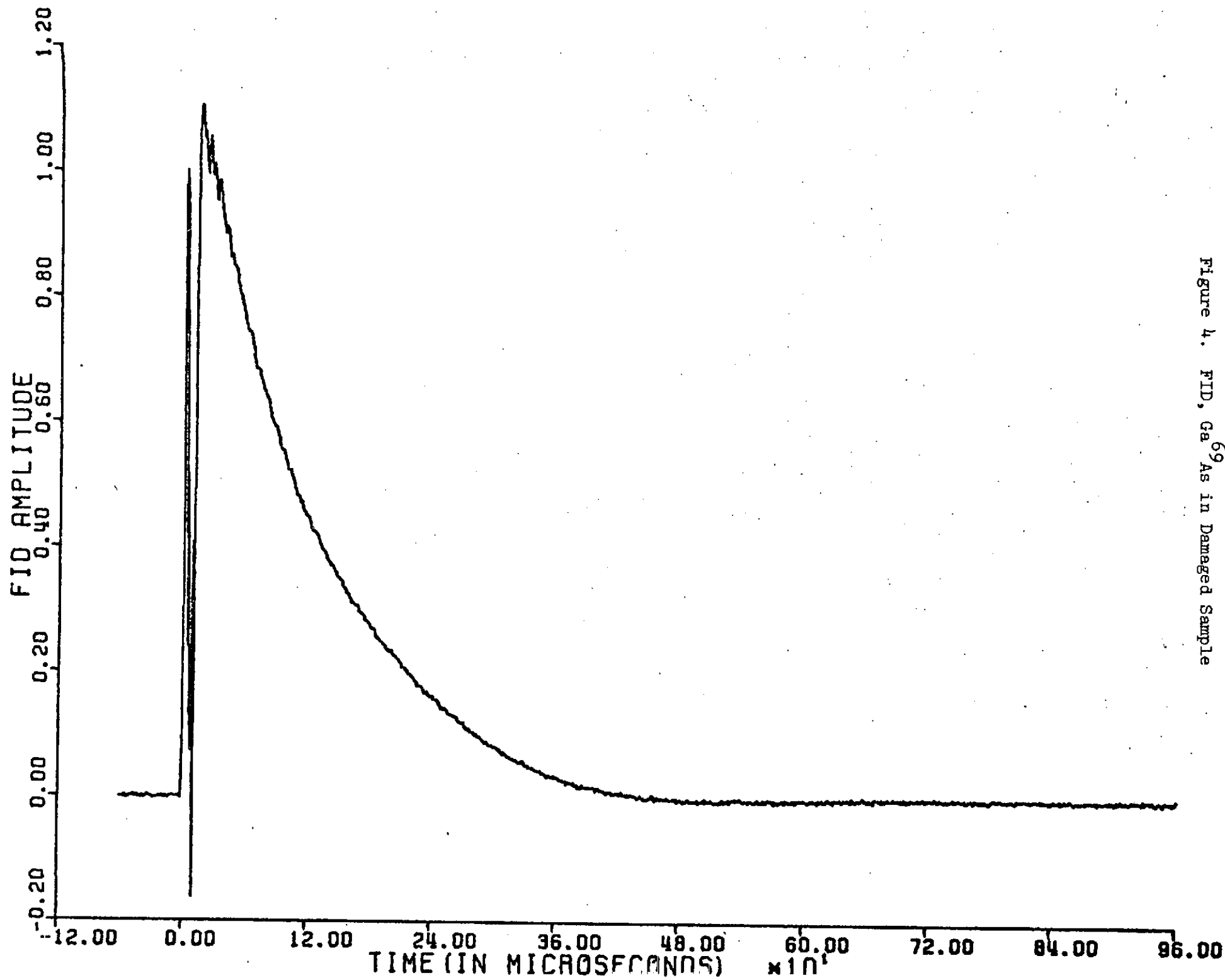


Figure 4. FID,  $\text{Ga}^{69}$  As in Damaged Sample



be about  $5 \times 10^{16} \text{ cm}^{-3}$ . This curve appears more exponential in character than Figure 3, and the oscillation is smaller.

Similar curves were obtained for these samples as a function of the orientation of the sample in the magnetic field. The data were transferred to magnetic tape, then processed in the William and Mary IBM 360 computer.

Least-squares best fits were obtained for these data, assuming a modified form of the function given in Eq. (23). The form used was

$$G(t) = C(.6 e^{-t^2/2\tau_1^2} + .4 e^{-t^2/2\tau_2^2}) \frac{\sin bt}{bt} . \quad (25)$$

The essential difference is that the experimental results are expressed in the time domain, while Eq. (23) is in the frequency domain. The curve fitting is quite successful, as seen in Figures 5 and 6.

In order to compare the theory to these results, Eqs. (18) and (24) are used. The second moments of the experimental results are found from  $\frac{\partial^2 G}{\partial t^2} \Big|_{t=0}$ .

Figures 7 and 8 display the experimental second moments of the two crystals as a function of crystal orientation in the magnetic field. Also shown are the Van Vleck calculations of the magnetic dipole-dipole second moment, and a best fit curve of the functional form

$$\langle \Delta \nu^2 \rangle = A + B f(\theta) \equiv A + B \left[ 2 \cos^2 \theta - \frac{3}{2} \cos^4 \theta \right] . \quad (26)$$

This function is similar to Eq. (18), and should have the correct angular variation for all of the NMR line broadening mechanisms present in this material.

Figure 5. FID,  $\text{Ca}^{69}\text{As}$  (Undamaged), and Best Fit Curve of Eq. (25)

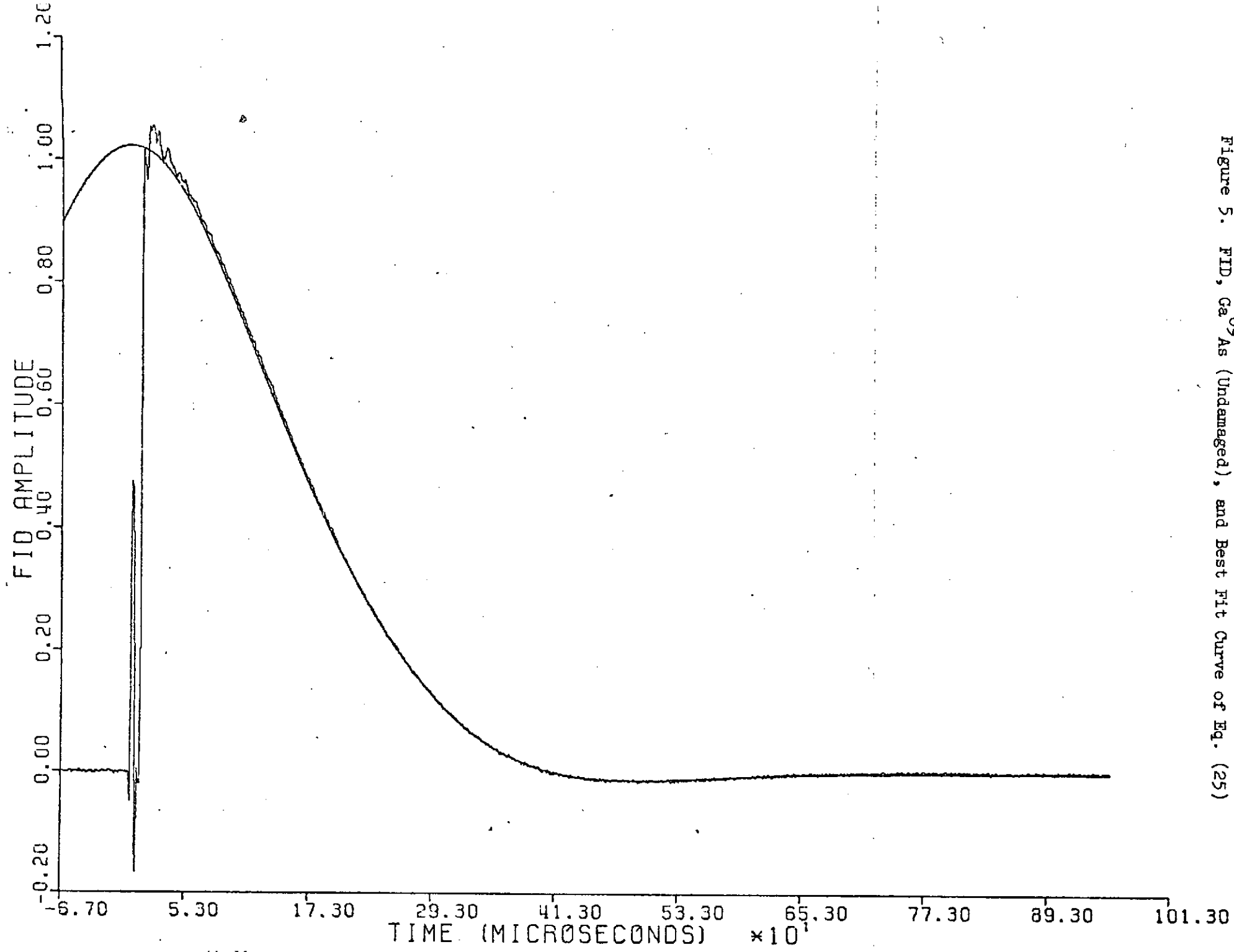


Figure 6. FID,  $\text{Ga}^{69}\text{As}$  (Damaged), and Best Fit Curve of Eq. (25)

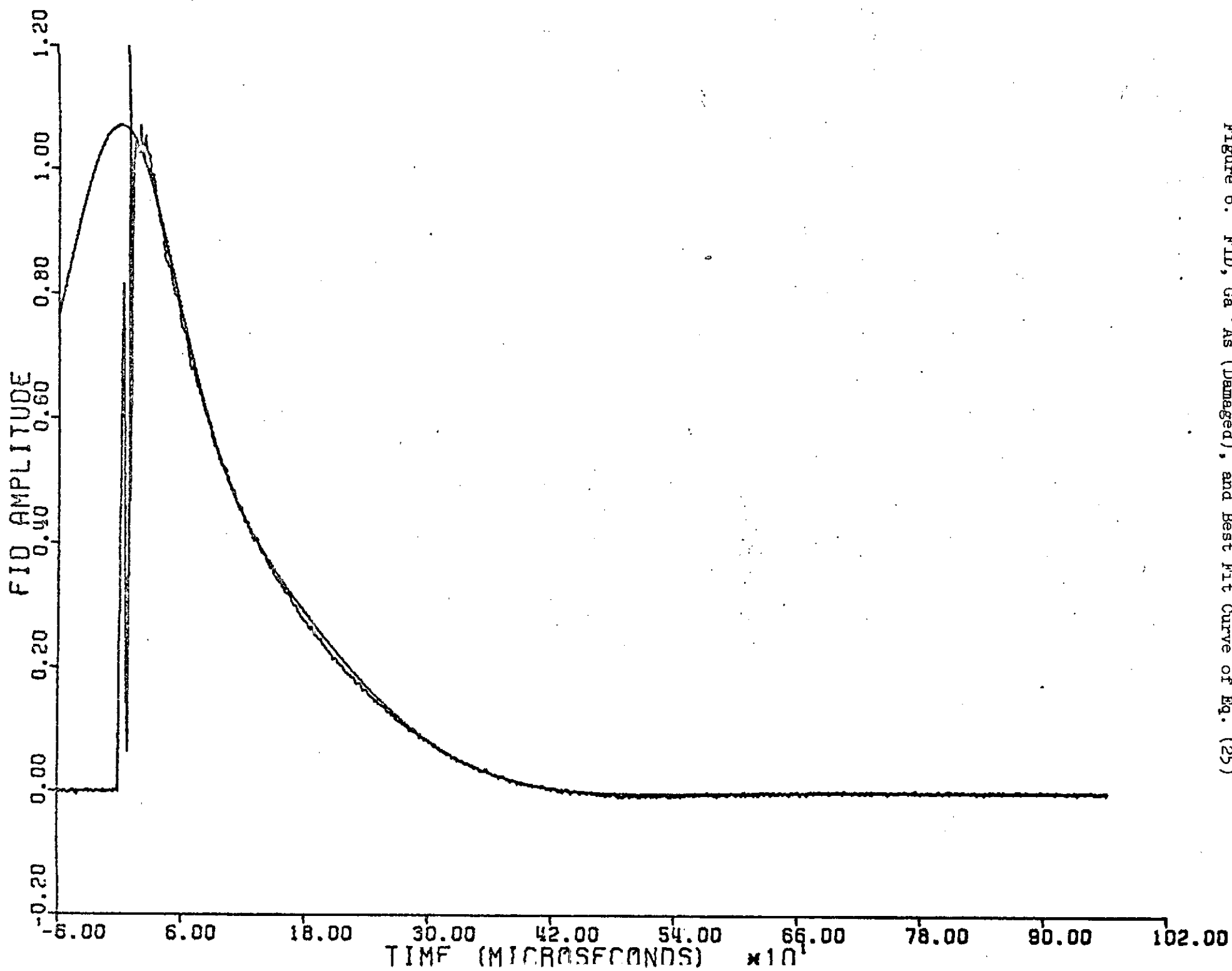


Figure 7.  $^{69}\text{Ga}$  As (Undamaged) Second Moments vs. Orientation, and Best  
Fit Curve of Eq. (26) 25

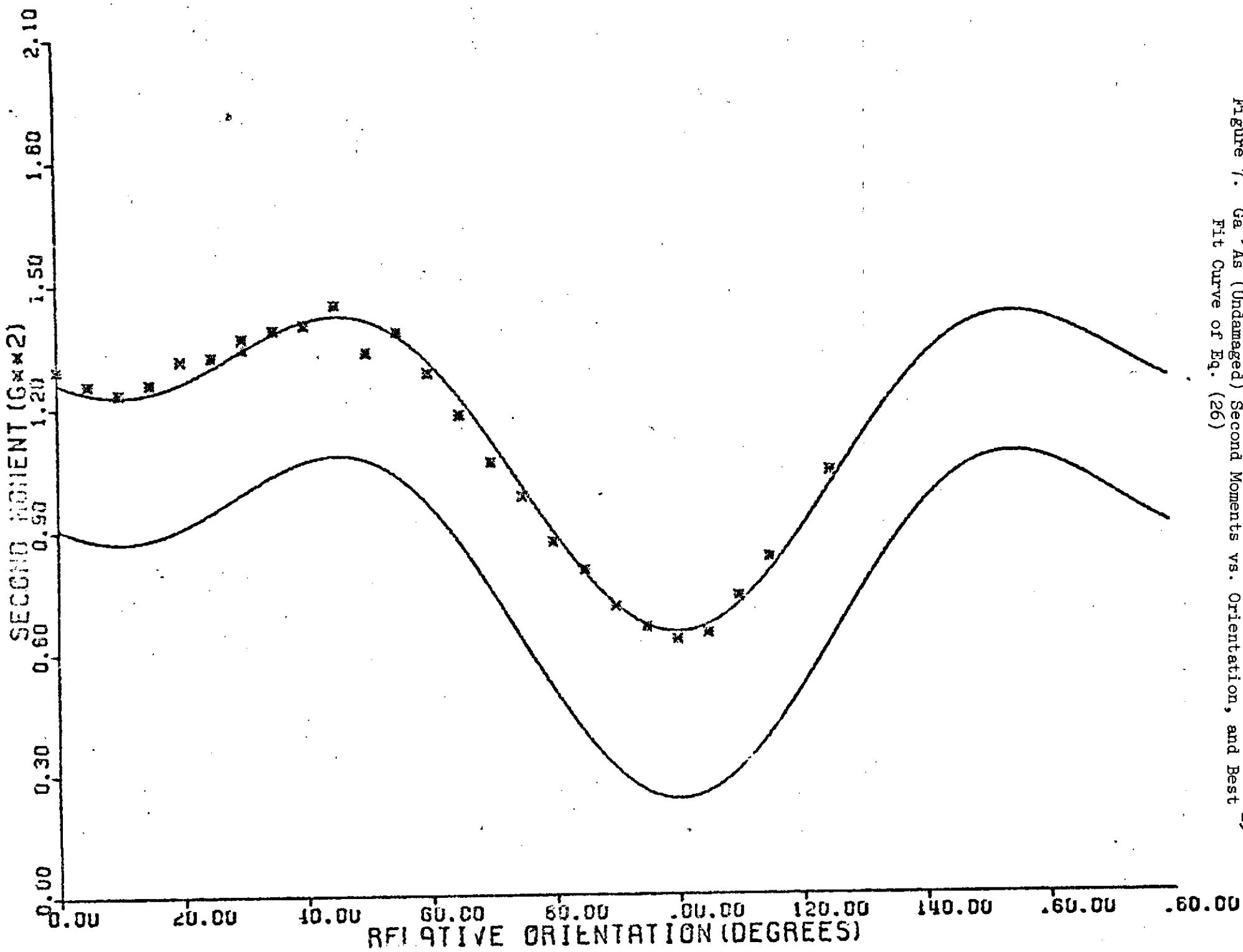
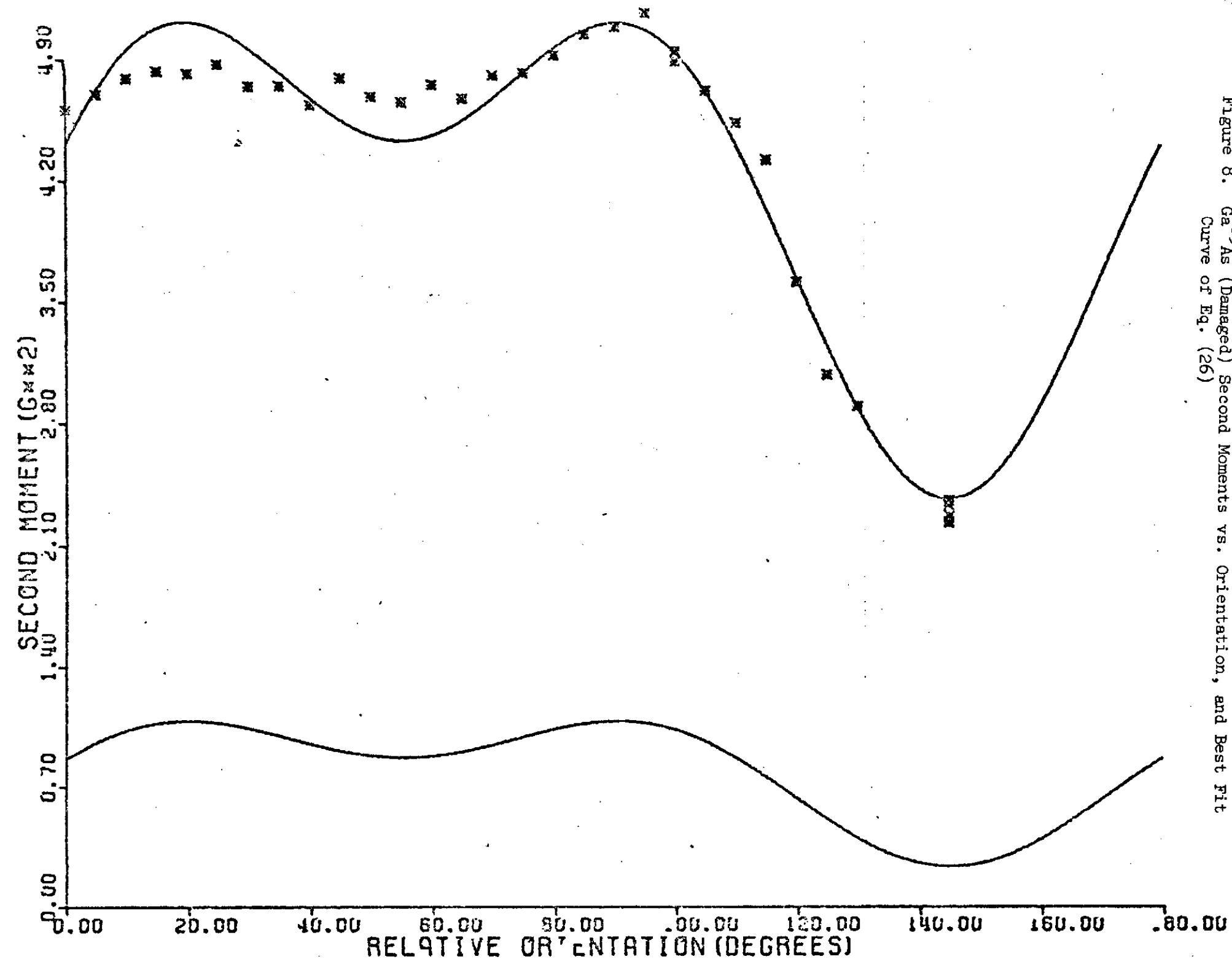


Figure 8.  $\text{Ga}^{69}\text{As}$  (Damaged) Second Moments vs. Orientation, and Best Fit Curve of Eq. (26)



### Line broadening mechanisms

As discussed by Sundfors,<sup>2</sup> there are three line broadening mechanisms important to the data taken in these samples. They are: magnetic dipole-dipole, electric quadrupole with impurity-caused field gradients, and nuclear pseudo-exchange interactions. In the undamaged crystal, our calculation of dipole-dipole and exchange effects are in agreement with Sundfors. Further, the exchange effects are not different in the damaged crystal. The remaining questions are thus: how does the dipole-dipole contribution vary with defect concentration; and more importantly, how sensitive is the quadrupolar broadening to the defect concentration?

The dipole-dipole interaction varies with defect concentration due to the first-order quadrupole frequency shift of the NMR  $3/2 \rightarrow 1/2$ ,  $-1/2 \rightarrow -3/2$  transitions. This shift makes part of the dipole-dipole hamiltonian non-secular, reducing the line broadening and causing an apparent narrowing of the resonance line. This effect is a small change - 10% or 20% - and we have discussed it in an earlier report on these experiments.<sup>1</sup>

Most of the change in second moments between Figures 7 and 8 is due to quadrupole mechanism proposed in Section II. The enormous change due to charged defects verifies our hypothesis that NMR is a sensitive tool for detection of these defects.

To be quantitative in this analysis, one must change the direction cosines expressed in Eq. (18) to the angle of orientation of a sample in the magnetic field. First, using the general expression  $n_x^2 + n_y^2 + n_z^2 = 1$  one can show

$$[(n_x n_y)^2 + (n_x n_z)^2 + (n_y n_z)^2] = \frac{1}{2} - \frac{1}{2} [n_x^4 + n_y^4 + n_z^4]$$

These samples were rotated about the  $\langle 110 \rangle$  axis (i.e. the  $\langle 110 \rangle$  axis is held perpendicular to the constant magnetic field.). Defining the angle between a  $\langle 1\bar{1}0 \rangle$  axis and the magnetic field as  $\theta$ , Eq. (18) becomes

$$\overline{\Delta\nu^2} = \frac{2\pi}{3} \rho_1 \frac{e^2 Q^2 e^{*2} R^2}{a h^2 \epsilon^2} f(\theta), \quad (18')$$

where  $f(\theta)$  is the function defined in Eq. (26). The quadrupole contributions to the second moment have the same functional form as the angular dependent part of the dipole-dipole contributions. For example, the Van Vleck calculation of dipole-dipole broadening for  $\text{Ga}^{69}\text{As}$  gives

$$\langle \Delta\nu_{69}^2 \rangle_{vv} = .299 + 1.33 f(\theta) \quad (kH_3^2). \quad (27)$$

In order to find the quadrupole contribution  $\overline{\Delta\nu^2}$  to the composite second moment  $\sigma_c^2$ , one must subtract all other contributions from the composite moment, as shown by Eq. (24). Adding Sundfors' value of the isotropic exchange coupling,  $\langle \Delta\nu_{69}^2 \rangle_{ex} = .265 kH_3^2$ , to the dipole term given by Eq. (27), the sum of terms other than quadrupolar becomes

$$\sigma_o^2 = \langle \Delta\nu_{69}^2 \rangle_{ex} + \langle \Delta\nu_{69}^2 \rangle_{vv} = .564 + 1.33 f(\theta). \quad (28)$$

The composite second moments for the undamaged crystal,  $(\sigma_c^2)_u$ , and the damaged crystal,  $(\sigma_c^2)_d$ , are given by the best fit values for the parameters A and B in Eq. (26). The curves shown in Figures 7 and 8 are

$$(\sigma_c^2)_u = .679 + 1.22 f(\theta) \quad (\text{undamaged}), \quad (29)$$

and

$$(\sigma_c^2)_d = 2.48 + 4.30 f(\theta) \quad (\text{damaged}).$$

Using Eqs. (24), (28), and (29), one finds

$$\overline{\Delta v_u^2} = \frac{(\sigma_c^2)_u - \sigma_o^2}{.6} = .192 - .18 f(\theta),$$

and

$$\overline{\Delta v_D^2} = 3.20 + 4.95 f(\theta). \quad (30)$$

If no other broadening mechanisms are present, the coefficient of  $f(\theta)$  in Eq. (30) arises from quadrupolar broadening. Two aspects of Eq. (30) make this attribution suspicious - the existence of an isotropic contribution, and the negative coefficient of  $f(\theta)$  for the undamaged crystal. The latter implies that the dipolar and isotropic exchange interactions give contributions larger than the experimentally measured moments. More recent data have shown that a pseudo-dipolar exchange interaction is present. This will be reported at a later date. For now, for order-of-magnitude purposes, we will assume the coefficient 4.95 in the damaged sample is due entirely to quadrupolar broadening.

The angular dependent part of  $\overline{\Delta v_D^2}$  gives us  $\overline{\Delta v^2}$  in Eq. (18').

Using the values  $a = \sqrt{3}a_0/4$  (assuming an As defect),  $\epsilon(\omega=0) = 12.5$ ,  $e^* = e$ ,  $R = 10^{10} \text{ cm}^{-1}$ , and  $Q$  from Table I, we calculate  $\rho_I = 2.5 \times 10^{15} \text{ cm}^{-3}$ .

This value is an order of magnitude smaller than that predicted by extrapolation from the data of Pearson, *et.al.*<sup>11</sup> ( $\rho_I = 5 \times 10^{16} \text{ cm}^{-3}$ ). Considering the crude analysis here, this discrepancy is not at all disturbing. The important point is that we have easily detected a defect concentration that is lower by a factor of at least 100 from previous measurements.

#### More Recent Data and Analysis

During this past summer, considerable additional data were taken.  $\text{Ga}^{69}\text{As}$ ,  $\text{Ga}^{71}\text{As}$ , and  $\text{GaAs}^{75}$  resonances were observed as a function of crystal orientation; for an undamaged, pure crystal, a crystal doped with Si (carrier concentration  $4 \times 10^{16} \text{ cm}^{-3}$ ), and pure crystals heated to  $500^\circ\text{C}$ ,  $600^\circ\text{C}$ , and



700°C and then quenched at room temperature. Signals were observed carefully immediately after quenching in order to observe any annealing effects.

Using all three resonances, one can calculate the contributions of all broadening mechanisms. The quadrupole broadening thus calculated gives impurity concentrations that generally agrees in magnitude with the data of Pearson et al.,<sup>11</sup> but at even lower concentrations than cited here.

As the analysis of these data is completed, and the results prepared for publication, N.A.S.A. will be sent copies as addenda to this report.

# FOOTNOTES

1. R. Hester, A. Sher, and J. F. Soest, Bull. Am. Phys. Soc. 17, 332 (1972).
2. R. K. Sundfors, Phys. Rev. 185, 458 (1969).
3. R. Kubo and T. Nagamiya, Solid State Physics, (McGraw-Hill, 1969). p. 690.
4. D. Gill and N. Bloembergen, Phys. Rev. 129, 2398 (1963).
5. E. H. Rhoderick, J. Phys. Chem. Solids 8, 498 (1958).
6. A. Abragam, The Principles of Nuclear Magnetism, (Oxford, 1961), p. 126.  
V. Jaccarino, J. G. King, R. A. Satten, and H. H. Stroke, Phys. Rev. 94, 1798 (1954).
7. For comparison, we can examine Sundfors's theoretical model. He sets  $\epsilon = 1$ ,  $e^* = e$  and then computes  $\overline{\Delta v_s^2}$  from Eq. (10) by setting  $r$  equal to one-half the average distance between impurities,  $r = 1/2(3/4\pi\rho_I)^{1/3}$ , and averaging over  $\theta$ . This yields:

$$\begin{aligned}\overline{\Delta v_s^2} &= \frac{4e^4 Q^2 R^2}{h^2 (3/4\pi\rho_I)^{4/3}} \left[ (n_x n_y)^2 + (n_y n_z)^2 + (n_x n_z)^2 \right] \frac{1}{\pi} \int_0^\pi \cos^2 \theta d\theta \\ &= 2 \left( \frac{4\pi\rho_I}{3} \right)^{4/3} \frac{e^4 Q^2 R^2}{h^2} \left[ (n_x n_y)^2 + (n_y n_z)^2 + (n_x n_z)^2 \right].\end{aligned}$$

Using his experimental values of  $\overline{\Delta v_s^2}$  he calculated values of  $R$  that differ from other experimental values obtained by more direct means by a factor of three. While Sundfors's expression for  $\overline{\Delta v_s^2}$  has the correct angular dependence, there is no logical reason to expect it to produce the correct numerical results.

8. J. D. Ellett, Jr., M. G. Gibby, U. Haeberlen, L. M. Huber, M. Mehring, A. Pines, and J. S. Waugh, Advan. Magnetic Resonance 5, 117 (1971).

9. I. J. Lowe and C. E. Tarr, J. Sci. Instrum. (Series 2) 1, 320 (1968).
10. D. R. Torgeson, Rev. Sci. Instrum. 38, 612 (1967).
11. G. L. Pearson, H. R. Potts, and V. G. Macres, Proceedings of the Seventh International Conference on the Physics of Semiconductors, Damage in Semiconductors, (Dunod Cie, Paris, 1965), p. 197.

## Appendix A

The article following this page has been submitted to the Review of Scientific Instruments.

## Appendix B

Articles in preparation:

"Asynchronous Pulse Programmer for use with a Pulsed Nuclear Magnetic Resonance System", R. K. Hester, M. Schmidt, and J. F. Soest.

"A Minicomputer-Based High Speed Signal Averaging System", L. Botten, R. K. Hester, and J. F. Soest.

"Pulsed NMR Detection of Low Concentrations of Charged Defects in III-V Semiconductor Crystals", R. K. Hester, A. Sher, and J. F. Soest.

A Simple Computer Interface for Write-Only  
Parallel Data Transfers from the PDP-8/E\*

R. K. Hester and J. F. Soest

Department of Physics  
College of William and Mary  
Williamsburg, Virginia 23185

\*Supported by NASA Grant No. NGR-47-006-050.

## Abstract

A simple and inexpensive computer interface for write-only parallel data transfers from a Digital Equipment PDP-8/E minicomputer equipped with a KA8-E Positive I/O Bus to some peripheral device is described. The data transfer is under program control and is thus versatile enough to transfer data to a number of devices. The application discussed here is a data transfer to magnetic tape using a Cipher Model 100 incremental tape drive, for later processing by a large computer.

It is often advantageous to collect data using a laboratory minicomputer and then to transfer the data to a larger computer for analysis. In this laboratory, signal averaged pulsed NMR data are recorded on IBM compatible 9 track magnetic tape by our Digital Equipment Corp. (D.E.C.) PDP-8/E, using the interface described here. The interface allows parallel data transfer under program control and is able to couple the PDP-8/E through the Positive I/O Bus KA8-E to many devices merely by changing the output cable.

We record data temporarily at the end of each run using a Tennecomp TP-1375 cartridge recorder, and transfer it as a group to IBM compatible tape at a later time. Thus the tape drive is only occasionally needed and can be shared with other research groups. In addition, punched paper tape that is used by many laboratory instruments can be read into the PDP-8/E through the associated teletype, converted to the appropriate format, and transferred to the magnetic tape.

The circuit design, shown in Figure 1, requires eleven integrated circuits. Three MC3001 are used to buffer the data, preventing possible loading and cable noise problems. As designed, data are always present on the peripheral inputs, but if necessary the twelve AND gates could be enabled by a buffered input/output pulse (BIOP) from the KA8-E.

An eight input NAND gate (MC3015) detects the correct device code (as designed,  $2^4_8$ ) specified by the buffered memory bits 3 through 8 (BMB 03-08). The NAND gate output enables the instruction decoder, a one-of-eight decimal decoder (MC4048). This design uses only the instructions binary coded 1 through 4 by BMB 09-11. Coincidence of an instruction decoder output and a BIOP pulse on the input of one of four AND gates (MC3001) executes the instruction.

Two instructions may assert the KA8-E SKIP L signal (in turn causing the PDP-8/E to skip the next program step). The peripheral BUSY signal (after inversion) inhibits BIOP 1 from asserting SKIP L if the program interrogates the BUSY status (instruction 1) while the peripheral is busy. In addition, if the peripheral detects an error, a positive level on one of four inputs is inverted and passes through the AND gate (MC3011). This allows BIOP 2 to assert SKIP L when the program interrogates the error condition (instruction 2). Four lamps and drivers (MC858) are used to identify the error. Open collector NAND gates (N8881) assert the SKIP L line. All inverters are in MC3008 hex inverter packages.

Instruction 3 causes a STEP/WRITE action by the tape drive. Finally, when the data transfer is complete, instruction 4 causes the tape drive to write an inter-record gap (IRG).

The External Bus cabling plugs into a D.E.C. H803 connector block. This interface uses half of a D.E.C. W979 module. The output cabling consists of twisted pairs anchored to another module that plugs in an adjacent slot in the block.

The recording program depends on the type of peripheral. Most parallel data transfers can be done with a combination of the four instructions given here. For example, this same interface is being used to transfer data to a Digi-Data Model 1700 synchronous tape drive and formatter, and directly to an IBM-360 equipped with a special IBM 2972 Scientific Interface Control unit.

Copies of the software, both the PDP-8/E program and the Fortran program for reading the magnetic tape, are available from the authors.



# KA8-E EXTERNAL BUS

# CIPHER MODEL 100

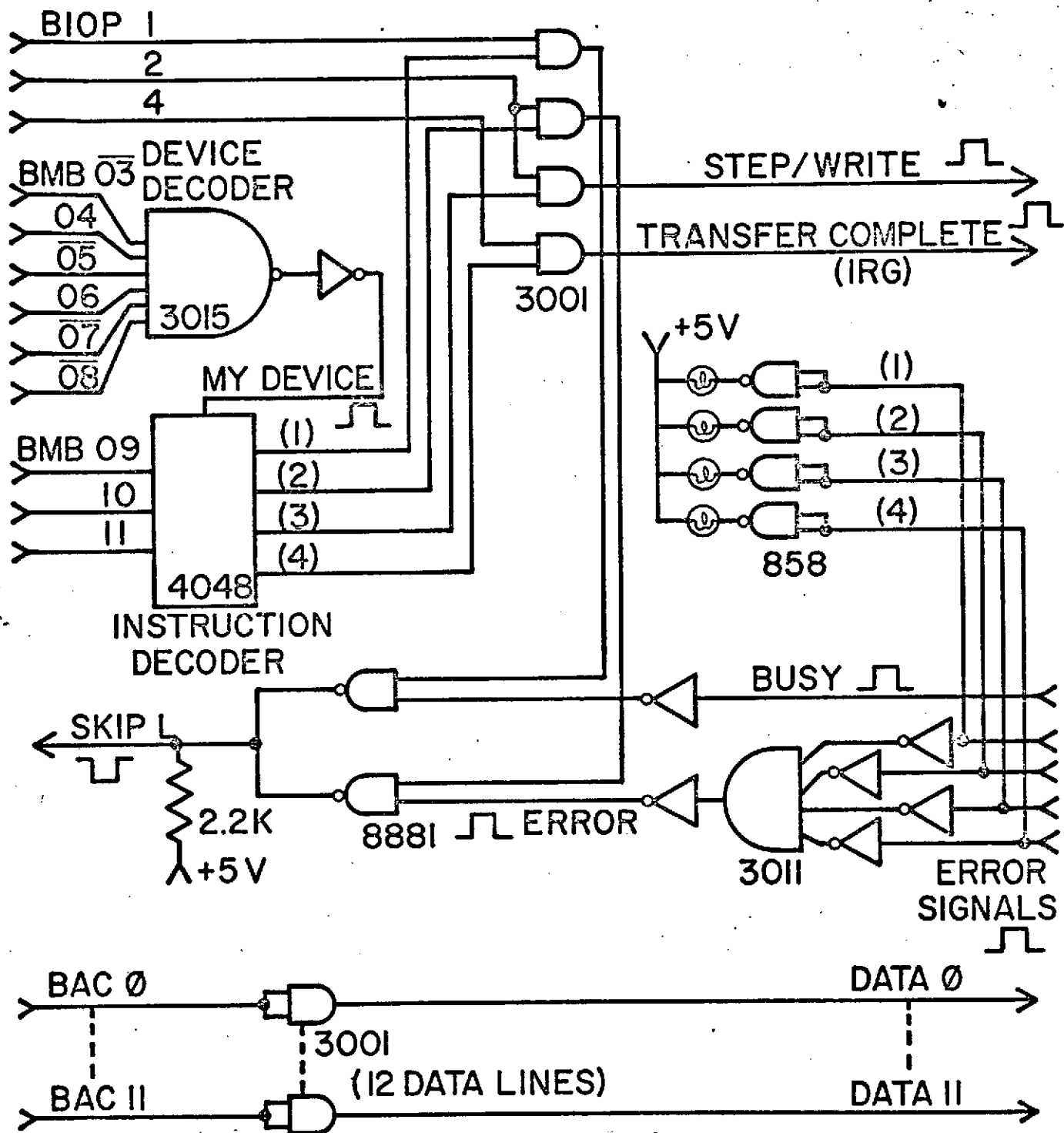


Fig. 1. Interface circuit diagram and interconnections. Cipher tape drive error signals are (1) broken tape, (2) tape end, (3) file protect, and (4) parity. Not shown are several inputs to the tape drive that must be grounded for write-only operation.

NMR Detection of Charged Defects in GaAs\*<sup>†</sup>

R. K. Hester, A. Sher, and J. F. Soest

Department of Physics, College of William and Mary, Williamsburg, Virginia 23185

and G. Weisz

Department of Psychology, University of Colorado, Boulder, Colorado 80302

ABSTRACT

Pulsed NMR was used to detect charged defect concentrations as small as  $2 \times 10^{14} \text{ cm}^{-3}$ . An undoped type n single crystal of GaAs was cut into several samples, and NMR second moments were obtained as a function of magnetic field orientation for  $\text{Ga}^{71}$ ,  $\text{Ga}^{69}$ , and  $\text{As}^{75}$ . The orientationally dependent part of the  $\text{Ga}^{71}$  second moment is one half that expected from the dipolar interaction. An explanation is given based on interference between the dipolar and the negative pseudodipolar interactions. There is a contribution to the second moment due to the electric quadrupolar interaction between nuclei and the electric field gradient (efg) associated

with point charge like defects, and it is proportional to the defect concentration. Because there are three isotopes we can separately identify the quadrupolar and pseudodipolar second moments. In order to introduce crystalline defects, samples were held at a constant temperature ( $500^{\circ}\text{C}$ ,  $550^{\circ}\text{C}$ ,  $600^{\circ}\text{C}$ ,  $700^{\circ}\text{C}$ ) in evacuated tubes and quenched to room temperature. The increase in second moment is due to the increased quadrupolar contribution, and it establishes the defect density for each damaged sample. The pseudodipolar interaction is observed to be independent of damage. Our data indicate that the defects are located on the As nuclear sites. No annealing was observed.

\*Supported in part by NASA grants NGR-47-006-050 and NGL-47-006-055 and NSF grant GH-41082.

<sup>†</sup>Based on a dissertation submitted by one of the authors (R.K.H.) to the Department of Physics, College of William and Mary, in partial fulfillment of the requirements for the degree of Doctor of Philosophy.

## I. INTRODUCTION

In III-V compounds, the broadening of the nuclear magnetic resonance (NMR) line is due to four rigid lattice interactions. In particular, the NMR second moments of the three isotopic species in GaAs ( $\text{Ga}^{71}$ ,  $\text{Ga}^{69}$ , and  $\text{As}^{75}$ ) contain contributions from all four of these mechanisms.

The dipolar interaction is well understood, and its contribution to the NMR second moment may be calculated theoretically<sup>1</sup>. In 1957 Shulman, et al.<sup>2,3</sup> reported linewidths in undoped powder samples of GaAs larger than those expected from the dipolar interaction alone. The additional broadening was attributed to the indirect exchange interaction between unlike spin systems. This nuclear exchange interaction involves an indirect nuclear spin coupling<sup>4-6</sup> via the hyperfine interaction between the electronic and nuclear spins. Its magnitude depends mainly upon the s character of the electronic wave function at the nuclear positions. More recently, Sundfors<sup>7</sup> has observed linewidths in several III-V compounds using both NMR and nuclear acoustic resonance (NAR) techniques. He identified the exchange contribution to the second moments and, using the theory of Anderson<sup>6</sup>, the exchange coupling constants.

Another electron coupled interaction is the pseudodipolar interaction<sup>4</sup>. The role of this mechanism in the broadening of NMR lines in III-V compounds is not well established, but a large negative pseudodipolar effect (canceling some

dipolar broadening) has been observed in the  $P^{31}$  resonance in  $InP$ <sup>8</sup>. The pseudodipolar interaction will be required to explain the data reported here. In undamaged samples both the  $Ga^{69}$  and  $Ga^{71}$  NMR second moments are smaller than those predicted by the dipolar interaction alone. In this case, the sign of the pseudodipolar coupling constant may be unambiguously determined.

GaAs has a zinc blende structure. Thus, the efg at nuclear sites is zero unless there are lattice defects. Randomly located lattice defects cause a random efg at nuclear sites and broaden the NMR line. E. H. Rhoderick<sup>9</sup> observed the effects of substitutional impurities upon NMR line intensities. The intensity loss with increasing impurity concentration is due to quadrupolar broadening caused by the efg associated with the impurities. It was found that the efg associated with ionized donor or acceptor impurities is larger than that associated with strains produced by neutral impurities. The explanation of the sensitivity of the NMR line to the ionized impurities<sup>10</sup> required anomalously large antishielding factors on the order of 1000.

Gill and Bloembergen<sup>11</sup> reported a direct measurement of the coupling constant relating the components of an efg tensor to an applied homogeneous electric field. The efg induced at nuclear sites is caused partly by a distortion of the valence orbitals and partly by a relative displacement of the Ga and As sublattices. Taking both effects into account, the coupling constant was explained using antishielding factors of 24 and 30 for Ga and As, respectively. Since the induced efg is proportional to the electric field, its magnitude decreases as  $r^{-2}$  in the field of a point charge. In contrast, the direct efg

caused by a point charge decreases as  $r^{-3}$ . Thus the quadrupolar interaction is dominated by the induced efg. Using this induced quadrupolar interaction it is not necessary to introduce large antishielding factors to explain Rhoderick's data.

Sundfors<sup>7</sup> identified the electric quadrupolar contribution to the NAR linewidths in samples of known carrier concentration. Comparing his measured linewidths to those predicted by a simplified theory of the induced quadrupole interaction linewidth, in which the number of charge centers is set equal to the carrier concentration, he obtained order of magnitude agreement with the measurements of Gill and Bloembergen.

In this research we demonstrate that NMR linewidths can be used to detect low concentrations of charged defects in single crystals of GaAs. We have done this with careful measurements of NMR second moments as a function of magnetic field orientation for all three isotopic species. We identify individual contributions from the four broadening interactions; and, using an improved theory, we show that the first order quadrupolar contribution is proportional to the charged defect concentration. Thus the identification of the quadrupolar contribution to the second moment is a measurement of this concentration.

Defect concentrations in several samples were altered by subjecting the samples to thermal damage. The process was similar to that of Potts and Pearson<sup>12</sup>, but our damage temperatures were far lower, producing fewer defects (on the order of  $5 \times 10^{14} \text{ cm}^{-3}$ , compared to their  $10^{18} \text{ cm}^{-3}$ .) Using vapor pressure data we estimate the As vacancy concentration caused by As sublimation at elevated temperatures. In this estimate we assume that As molecules in the vapor phase are frozen

out of the lattice by the thermal quench. The vacancy concentration deduced from the vapor pressure data is more than an order of magnitude larger than the concentrations projected from Potts and Pearson's experiments. Our NMR measurements of the defect concentrations lie about mid-way between the two projections.

## II. THEORY

Consider two different nuclear-spin systems with nuclei having spin angular momentum  $\hbar \underline{I}$  and  $\hbar \underline{S}$ , and non-overlapping resonances. The resonance experiment is performed on the spins I. We assume that the resonance is broadened by the following four interactions: dipolar, pseudodipolar, exchange, and quadrupolar. The second moment of the resonance line is calculated from the expression given by van Vleck<sup>1</sup>

$$\langle \Delta H^2 \rangle = -\chi_I^{-2} \hbar^{-2} \text{Tr} [\mathcal{H}, \hat{I}]^2 / \text{Tr} [\hat{I}^2], \quad (1)$$

where  $\mathcal{H}$  is the system hamiltonian, and  $I$  is the total spin operator proportional to the observed magnetization.

Following the notation of Sundfors<sup>7</sup>, we write the system hamiltonian as

$$\mathcal{H} = \mathcal{H}_{0I} + \mathcal{H}_{0S} + \mathcal{H}_{DI} + \mathcal{H}_{DS} + \mathcal{H}_{DIS} + \mathcal{H}_{EI} + \mathcal{H}_{ES} + \mathcal{H}_{EIS} + \mathcal{H}_{PI} + \mathcal{H}_{PS} + \mathcal{H}_{PIS} + \mathcal{H}_{QI}, \quad (2)$$

where  $\mathcal{H}_{0I}$  and  $\mathcal{H}_{0S}$  are the Zeeman energies for the I and S spins, respectively. We may combine the truncated dipolar and pseudodipolar interaction<sup>13</sup> terms as

$$\mathcal{H}_{DI} + \mathcal{H}_{PI} = \hbar^2 \chi_I^2 \sum_{i>j} (1+B_{ij}) (3I_{iz}I_{jz} - \underline{I}_i \cdot \underline{I}_j) P_2(\theta_{ij}) r_{ij}^{-3}, \quad (3a)$$

$$\mathcal{H}_{DS} + \mathcal{H}_{PS} = \hbar^2 \chi_S^2 \sum_{i>j} (1+\tilde{B}'_{ij}) (3S_{iz}S_{jz} - \underline{S}_i \cdot \underline{S}_j) P_2(\theta_{ij}) r_{ij}^{-3}, \quad (3b)$$



$$\mathcal{H}_{\text{DIS}} + \mathcal{H}_{\text{PIS}} = k^2 \chi_I \chi_S \sum_{i,j} (1 + \tilde{B}_{ij}) I_{iz} S_{jz} P_2(\theta_{ij}) r_{ij}^{-3}, \quad (3c)$$

where  $B_{ij}$  is the pseudodipolar coupling constant for like spins I,  $\tilde{B}'_{ij}$  is the pseudodipolar coupling constant for like spins S,  $\tilde{B}_{ij}$  is the pseudodipolar coupling constant for unlike spins I and S, and  $\underline{r}_{ij}$  is the displacement vector from the  $i^{\text{th}}$  nuclear site. The second Legendre polynomial is written as  $P_2(\theta_{ij})$ , where  $\theta_{ij}$  is the angle between  $\underline{r}_{ij}$  and the Zeeman field. The exchange terms may be written

$$\mathcal{H}_{\text{EI}} = \sum_{i,j} A_{ij} \underline{I}_i \cdot \underline{I}_j, \quad (3d)$$

$$\mathcal{H}_{\text{ES}} = \sum_{i,j} \tilde{A}'_{ij} \underline{S}_i \cdot \underline{S}_j, \quad (3e)$$

$$\mathcal{H}_{\text{EIS}} = \sum_{i,j} \tilde{A}_{ij} I_{iz} S_{jz}, \quad (3f)$$

where  $A_{ij}$  is the exchange coupling constant for like spins I,  $\tilde{A}'_{ij}$  is the exchange coupling constant for like spins S, and  $\tilde{A}_{ij}$  is the exchange coupling constant for unlike spins I and S. The quadrupolar term  $\mathcal{H}_{\text{QI}}$  can be written

$$\mathcal{H}_{\text{QI}} = A \sum_j [3I_{jz}^2 - I_j(I_j+1)] V_{zzj}^2, \quad (3g)$$

where  $V_{zzj}$  is the efg at nuclear site j, and  $A = eQ_I [4I(2I-1)]^{-1}$ , where  $Q_I$  is the electric quadrupole moment of the spins I.

By combining Eqs. (1), (2), and (3) one obtains the expression for the NMR second moment

$$\begin{aligned} \langle \Delta H^2 \rangle = & 3I(I+1) \chi_I^2 k^2 \sum_j [(1 + B_{jj}) r_{jj}^{-3} P_2(\theta_{jj})]^2 + \frac{1}{3} S(S+1) \sum_j \tilde{A}_{jj}^2 + \\ & + \frac{4}{3} S(S+1) \chi_S^2 k^2 \sum_j [(1 + \tilde{B}_{jj}) r_{jj}^{-3} P_2(\theta_{jj})]^2 + \\ & + \frac{9}{5} [4I(I+1) - 3] A^2 \chi_I^{-1} \chi_S^{-2} k^2 \sum_j V_{zzj}^2. \end{aligned} \quad (4)$$

The lattice sums in the dipolar terms of Eq. (4) may be separated into two parts, one of which contains no pseudodipolar coupling constants. Consider just the dipolar sum for like spin broadening. This may be written

$$\sum_j [(1+B_{ij})r_{ij}^{-3}P_2(\theta_{ij})]^2 = \sum_j B_{ij}(2+B_{ij})r_{ij}^{-6}P_2^2(\theta_{ij}) + \sum_j r_{ij}^{-6}P_2^2(\theta_{ij}). \quad (5)$$

The first sum on the right side of Eq. (5) contains the pseudodipolar contribution to the second moment and the interference term between the dipolar and pseudodipolar interactions. The second sum is just the dipolar contribution in the presence of zero pseudodipolar interactions. This sum may be performed, and for the zinc blende lattice it has the form<sup>1</sup>

$$\sum_j r_{ij}^{-6}P_2^2(\theta_{ij}) = \frac{1}{8} [a + b(n_x^4 + n_y^4 + n_z^4)], \quad (6)$$

where  $n_x$ ,  $n_y$ , and  $n_z$  are the direction cosines of the Zeeman field in the crystalline coordinate system. When the sum is performed over nuclear sites on the fcc sublattice containing the spins I, Sundfors computes  $a=256 a_0^{-6}$  and  $b=-118 a_0^{-6}$ , where  $a_0$  is the lattice constant. For the non-resonant sublattice he computes  $a'=2491 a_0^{-6}$  and  $b'=-2390 a_0^{-6}$ .

If the magnetic field is rotated in the  $(1\bar{1}0)$  plane, and  $\theta$  is defined as the angle between the  $[110]$  direction and the Zeeman field, then

$$n_x^4 + n_y^4 + n_z^4 = 1 - f(\theta), \quad (7)$$

where  $f(\theta) = 2 \cos^2 \theta - \frac{3}{2} \cos^4 \theta$ . Combining Eqs. (6) and (7) we may write the dipolar sum in terms of  $f(\theta)$ ,

$$\sum_j r_{ij}^{-6}P_2^2(\theta_{ij}) = X + Y f(\theta), \quad (8)$$

where  $X = (a+b)/8$ , and  $Y = -b/8$ . The dipolar contribution to the NMR second moment thus contains an isotropic part,  $X$ , and a part dependent upon the magnetic field direction,  $Y$ .

We consider now the first sum on the right hand side of Eq. (5). The electron coupled pseudodipolar interaction is extremely short range<sup>5</sup>, and we assume that only nearest neighbors interact. Thus the first sum in Eq. (5) vanishes because it does not contain the nearest neighbor shell. However, the corresponding term in the expression for unlike dipolar broadening does contain the nearest neighbor shell. The coefficients  $\tilde{B}_{ij}$  are independent of  $\theta_{ij}$  and may be factored out of the sum. The pseudodipolar terms become

$$\hbar^2 \chi_s^2 \sum_j \tilde{B}_{ij} (2 + \tilde{B}_{ij}) r_{ij}^{-6} P_2^2(\theta_{ij}) = 2 \hbar^2 \chi_s^2 \tilde{B}_{NN} (2 + \tilde{B}_{NN}) (4/a\sqrt{3})^6 f(\theta), \quad (9)$$

where  $B_{NN}$  is the nearest neighbor pseudodipolar coupling constant. With this nearest neighbor approximation, the pseudodipolar terms have the same orientation dependence as the angular part of the dipolar contribution to the second moment, but there is no isotropic pseudodipolar contribution.

In order to evaluate the quadrupolar contribution to the second moment we require a specific model for the efg tensor. The efg associated with crystalline strain is much smaller than that caused by charged impurities<sup>7,9</sup> and may be neglected when both are present. Thus we assume that the efg is due entirely to the electric field of charged crystalline defects. The general tensor relationship between the components  $V_{ij}$  of the efg tensor and the electric field components  $E_k$  is given by<sup>11,14</sup>

$$V_{ij} = \sum_k R_{ijk} E_k, \quad (10)$$

where  $R_{ijk}$  is a third rank tensor. In the zinc blende crystalline coordinate system Eq. (10) may be written<sup>11</sup>

$$V = -R_{14} \begin{pmatrix} 0 & E_z & E_y \\ E_z & 0 & E_x \\ E_y & E_x & 0 \end{pmatrix}, \quad (11)$$

where  $R_{14}$  is the magnitude of the non-vanishing tensor components.

The component of  $V$  in the secular part of the quadrupole hamiltonian is  $\hat{n} \cdot V \cdot \hat{n}$ , where  $\hat{n}$  is the unit vector in the direction of the Zeeman field. We find

$$\hat{n} \cdot V \cdot \hat{n} = -2R_{14}(n_y n_z E_x + n_x n_z E_y + n_x n_y E_z). \quad (12)$$

Since most of the nuclei affected by a given impurity lie outside the first few near neighbor shells, we use the static macroscopic dielectric constant  $\epsilon$  to approximate the electronic screening.<sup>15</sup> Thus the electric field at a displacement  $r$  from a single impurity of effective charge  $e^*$  is

$$\underline{E} = e^* \underline{r} / \epsilon r^3. \quad (13)$$

Combining Eqs. (4), (12), and (13), we obtain an expression for the quadrupolar

contribution to the second moment for a single impurity

$$\langle \Delta H^2 \rangle_{Q,1} = \frac{36}{5} [4I(I+1)-3] \left( \frac{AR_{14}e^*}{\epsilon \gamma_I \hbar} \right)^2 \frac{1}{N} \sum_j r_j^{-6} (n_y n_z x_j + n_x n_z y_j + n_x n_y z_j). \quad (14)$$

Due to the lattice symmetry of GaAs, summations over terms  $x_j y_j$ ,  $x_j z_j$ , and  $y_j z_j$  vanish, and summations over terms  $x_j^2$ ,  $y_j^2$ , and  $z_j^2$  are equal. Using these and the properties of direction cosines we may rewrite Eq. (14)

$$\langle \Delta H^2 \rangle_{Q,1} = \frac{6}{5} [4I(I+1)-3] \left( \frac{AR_{14}e^*}{\epsilon \gamma_I \hbar} \right)^2 \frac{1}{N} \sum_j r_j^{-4} f(\theta). \quad (15)$$

We assume that the charged defects occur randomly on one sublattice. The efg at a nuclear site is the sum of contributions from each of the charged defects. From the central limits theorem,<sup>16</sup> the broadening due to  $N_I$  impurities is  $N_I$  times that due to a single impurity, and the quadrupolar second moment expression becomes

$$\langle \Delta H^2 \rangle_Q = \frac{6}{5} [4I(I+1)-3] \left( \frac{AR_{14}e^*}{\epsilon \gamma_I \hbar} \right)^2 \left( \frac{\rho_I}{\rho} \right) f(\theta) \sum_j r_j^{-4}, \quad (16)$$

where the ratio of defect density to nuclear density  $\rho_I/\rho$  has replaced the ratio  $N_I/N$ . This contribution has the same angular dependence as the pseudodipolar second moment. Both vanish when  $\theta = \pi/2$ , where the Zeeman field is aligned with the [001] direction.

We have calculated the lattice sum over  $r_j^{-4}$  in Eq. (16). The discrete sum was performed over a cube with an edge size of  $16a_0$ . An integral was performed over the remainder of the sample<sup>17</sup>. The result of this calculation is  $33.75 a_0^{-4}$  for impurities located on the same sublattice as the nuclear spins  $I$ , and  $63.31 a_0^{-4}$  for the impurities located on the other sublattice.

### III. EXPERIMENT

The experiment was performed on several type n single crystals of GaAs, sliced from a single undoped, boat grown ingot, purchased from the Monsanto company. The properties of the ingot were supplied by Monsanto as follows: resistivity,  $1.34 \times 10^4$  ohm-cm; carrier concentration,  $2.4 \times 10^{11}$  cm<sup>-3</sup>; electron mobility,  $2.7 \times 10^3$  cm<sup>2</sup>volt<sup>-1</sup>sec<sup>-1</sup>; and etch pit density,  $4.2 \times 10^4$  cm<sup>-2</sup>. A 50 micron diamond saw was used to cut the ingot into several samples of nearly equal size, about 0.5cm by 0.5cm by 1.0 cm. A type n silicon doped sample purchased from Electronic Materials Corporation was also studied. Its properties as measured by the manufacturer, were: resistivity, .03 ohm-cm; carrier concentration,  $4 \times 10^{16}$  cm<sup>-3</sup>; electron mobility,  $5 \times 10^3$  cm<sup>2</sup>volt<sup>-1</sup>sec<sup>-1</sup>; and etch pit density,  $8 \times 10^4$  cm<sup>-2</sup>.

The free induction decay (FID) following a single 90° pulse was observed for the three isotopes in each of the samples as a function of magnetic field orientation. The  $[1\bar{1}0]$  axis of the sample was oriented perpendicular to the magnetic field, and changes in the magnetic field orientation were accomplished by rotating the sample about this  $[1\bar{1}0]$  axis. In this way, the major crystalline symmetry axes ( $[001]$ ,  $[110]$ , and  $[111]$ ) could be aligned with the magnetic field. After a sample was studied, it was subjected to thermal damage, and each isotope was studied again in the same manner.

In order to introduce a known defect concentration in the samples, each was thermally damaged following the method of Potts and Pearson<sup>12</sup>. In that work the crystals were held at a constant elevated temperature ( $1000^{\circ}\text{C}$  to  $1200^{\circ}\text{C}$ ) in an evacuated vessel for 24 hours and then quenched to  $0^{\circ}\text{C}$  in less than 0.2 seconds. Vacancy concentrations were then determined by the Kossel line technique<sup>12,18</sup>. In our experiment much lower prequench temperatures were used ( $500^{\circ}\text{C}$  to  $700^{\circ}\text{C}$ ), thus introducing lower defect concentrations. In addition, due to the size of our samples, a rapid quench would cause macroscopic damage, so a much longer quenched period of 10 to 15 minutes was used. Ionic mobilities in GaAs near room temperature are quite low<sup>19</sup>, so the vacancy concentration caused by sublimation of As atoms is not expected to depend upon the period of the quench. However, Frenkel pairs may recombine quickly, and a longer quench period might substantially reduce their concentration. Room temperature annealing of damaged samples was observed by Potts and Pearson, and it was interpreted, in part, as due to the recombination of Frenkel pairs. No annealing was observed in our samples, so any Frenkel pairs must have already recombined. In addition, after the quench a metallic film remained on the vycor vessel. Chemical analysis failed, but from vapor pressure data we are convinced that it was As. It is concluded that this slow thermal quench generates As monovacancies.

NMR measurements were made with a pulsed NMR system shown in block diagram form in Fig. 1. All measurements were made at a fixed frequency of 14.4 MHz, with the appropriate magnetic field supplied by a Varian V-3900 electromagnet and power supply equipped with Mark I Fieldial stabilization. The rf system, with few exceptions, is very similar to that described by Ellett, et al.<sup>20</sup> as

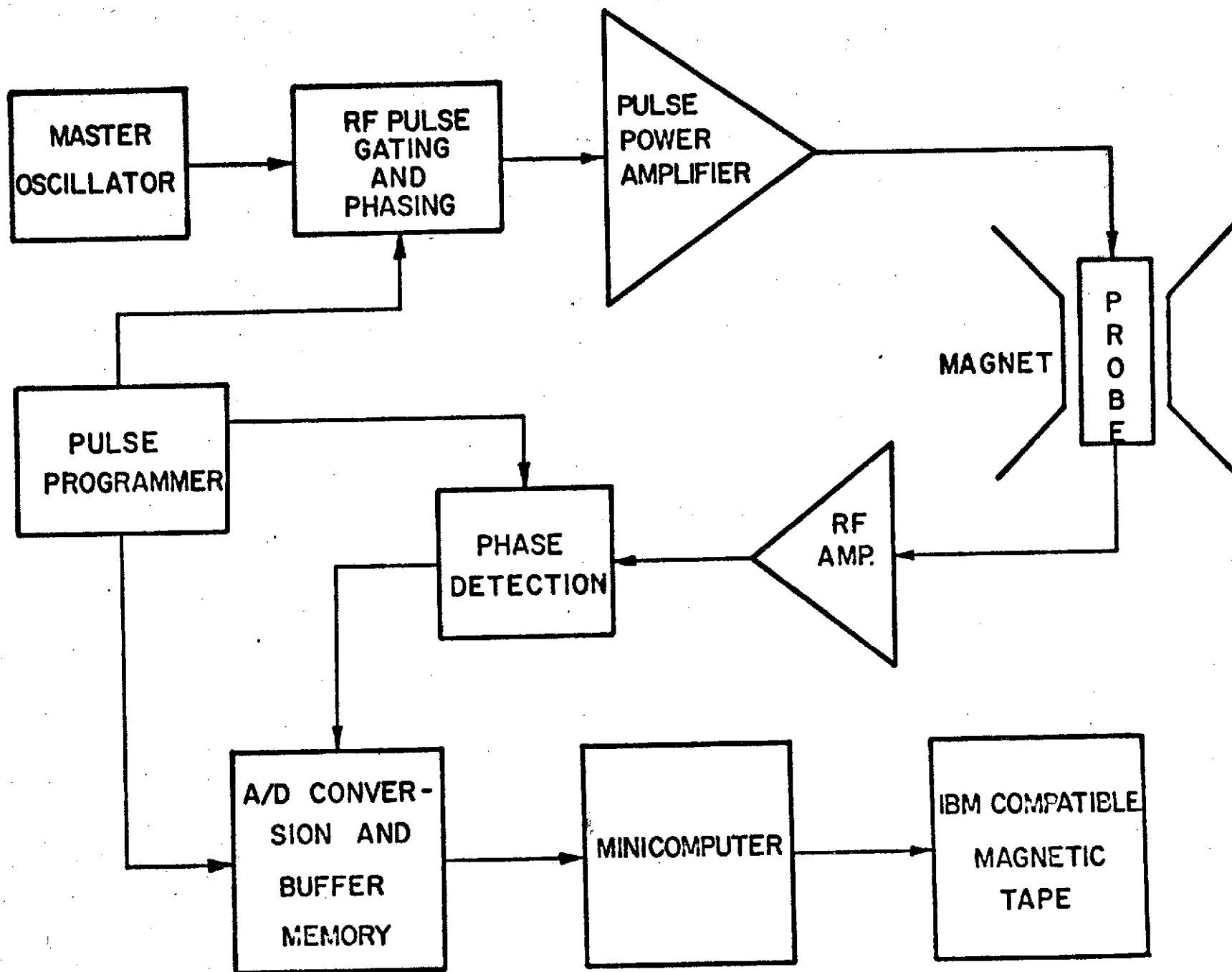


Figure 1 Block diagram of pulsed NMR apparatus.



spectrometer B. Our gated power amplifier, however, is an NMR Specialties Model P-103R. Also, the signal duplexer and preamplifier are those described by Lowe and Tarr,<sup>21</sup> modified for a 50 ohm system. A single coil, series tuned probe was used. At resonance the probe impedance was 50 ohms with a quality factor of approximately 5.

Since the sample is piezoelectric it produced an unwanted transient signal following the rf pulse. Without special precautions this distorted approximately the first 100 microseconds of the FID. It was suggested that such noise may be damped by placing the sample in contact with a fluid of appropriate viscosity. However, it was easier, and just as effective, to surround the sample by a Faraday shield. The mylar strip was removed from a metallized mylar capacitor, enclosed in insulating tape, and wound closely around the sample coaxially with the rf coil. This reduced both the amplitude and the duration of the piezoelectric noise by an order of magnitude.

Control of the experiment timing is provided by a pulse programmer designed and constructed in this laboratory. Its operation is based upon a 256 bit random access memory divided into 16 eight bit words. On execution, each word performs a single step of a pulse sequence, either a pulse or a delay. Pulse and delay durations can be controlled either digitally (using a 10 MHz crystal oscillator) or continuously (using 9601 monostable multivibrators). Two internal step counters as well as a minicomputer interface allow the programmer to control almost any pulsed NMR experiment.

The signal to noise ratio (S/N) of the FID following each  $90^\circ$  pulse was

approximately 10, too small for accurate determination of the linewidths. So 5000 FID's were signal averaged to yield a S/N of over 700.

The FID undergoes analog-to-digital conversion in an 8 bit converter, a modified Computer Labs Model HS-802, at a rate of up to 5 MHz. Because this rate is too great for direct computer storage, the data for a single FID (1024 eight bit words) are stored in a buffer memory. Subsequent transfer to a Digital Equipment Corp. PDP 8/e minicomputer takes place during the NMR longitudinal relaxation time,  $T_1$ , at a rate set by the computer. The computer maintains storage of the most recent FID and the accumulated sum. Either of these may be displayed on an oscilloscope during  $T_1$ . When 5000 FID's have occurred, the computer transfers the accumulated data onto 9 track, industry compatible magnetic tapes. The analysis of the data was performed with an IBM 360/50 computer.

#### IV. ANALYSIS

Lowe and Norberg<sup>22</sup> have shown that the moments of the NMR line can be determined from the time derivatives of the FID at  $t=0$  by using the relation

$$\langle \Delta \omega^{2n} \rangle = \frac{(-1)^n}{g(0)} \left( \frac{d^{2n} g(t)}{dt^{2n}} \right)_{t=0}, \quad (17)$$

where  $\langle \Delta \omega^{2n} \rangle$  is the  $2n^{\text{th}}$  moment and  $g(t)$  is the FID. However, the  $t=0$  point is precisely in the center of the rf pulse<sup>23</sup>, and the FID derivatives cannot be measured there directly. One method of obtaining second moments from the FID is to fit the visible part to an analytic function and to extrapolate back to  $t=0$  in order to evaluate the derivatives. The accuracy of this method, of course, depends upon the ability of the function to describe the FID.

We used a least squares fitting routine<sup>24</sup> to fit the FID with two functions. The Abragam function

$$g(t) = \exp(-\alpha^2 t^2 / 2) \sin \beta t / \beta t \quad (18)$$

was found to approximate the  $F^{19}$  free induction decay in  $\text{CaF}_2$  very well.<sup>25</sup> Our data appear qualitatively similar to the fluorine FID. However, when the Abragam function was fit to GaAs FID's, there were systematic deviations. Fig. 2 shows the generally unsatisfactory character of the fits of this function.

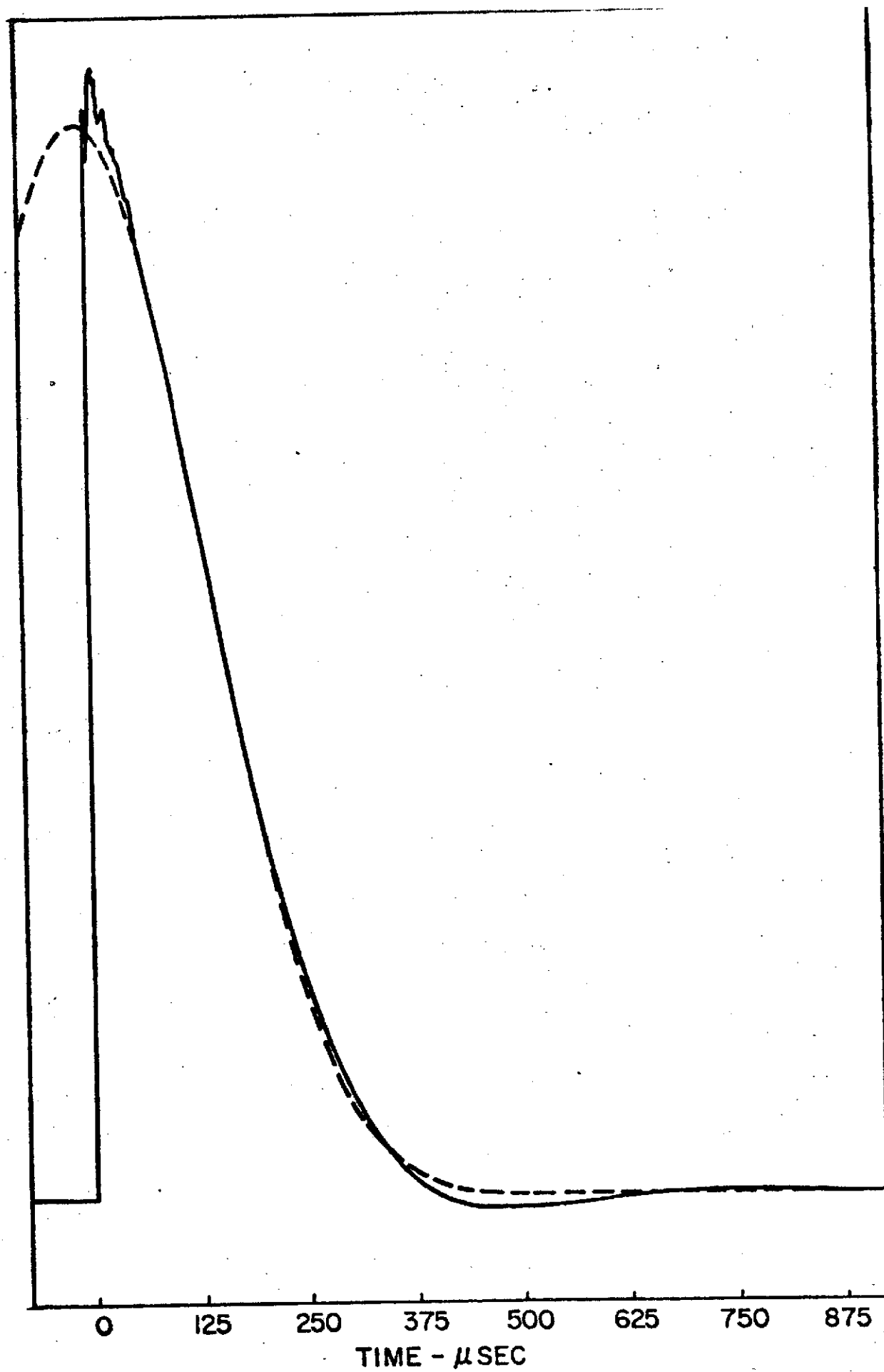


Figure 2  $\text{Ga}^{69}$  FID and best functional fit using Abragam function.

$F^{19}$  has spin  $\frac{1}{2}$  and so zero quadrupole moment. Thus one would expect the GaAs FID shapes to be modified by quadrupolar broadening. For half odd integral spins the first order effect of an efg is to leave the transition between the  $1/2$  to  $-1/2$  energy levels unchanged and to split the other transitions into satellites. If the efg is random this leaves the central component of the line unbroadened while the remainder of the line broadens. Thus the FID has a fast decaying component arising from the satellites and a slower decaying component arising from the central component. In the case of spin  $I=3/2$  nuclei, the satellite lines make up 60% and the central component lines the other 40% of the total resonant absorption. Thus the FID can better be described by a sum of two Abragam functions. The function

$$g(t) = [I_1 \exp(-\alpha^2 t^2/2) + I_2 \exp(-\delta^2 t^2/2)] \sin \beta t / \beta t \quad (19)$$

describes the GaAs FID very well, as shown in Figs. 3 and 4. The angular frequency second moment of a FID described by Eq. (19) is  $\frac{1}{3}\beta^2 + (I_1\alpha^2 + I_2\delta^2)/(I_1 + I_2)$ .

Based on the above reasoning, more adequately discussed in the Appendix, one expects to find  $I_1/I_2=2/3$  and  $\alpha < \delta$ . However this is not always the case. We find that the ratio  $I_1/I_2$  departs from its expected value with increasing quadrupole interaction. The quadrupole moments as shown in Table I obey the inequality  $Q_{75} > Q_{69} > Q_{71}$ . In all samples the As<sup>75</sup> FID (for  $\theta \neq \pi/2$ ) is described by Eq. (19) with  $I_1/I_2 > 2/3$ . This is also true of the Ga<sup>69</sup> and, to a lesser extent, the Ga<sup>71</sup> FID in samples with large defect concentrations.

One reason for this departure is our choice of the Abragam function as the functional form of the FID in the absence of the quadrupole interaction.

TABLE I. RELEVANT NUCLEAR PROPERTIES<sup>a</sup>

Isotope	Natural Abundance (%)	I	Magnetic Moment ( $\mu_N$ )	Electric Quadrupole Moment (barns)	$R_{14}^b$ ( $10^{10} \text{ cm}^{-1}$ )
Ga <sup>71</sup>	39.8	3/2	2.5549	.12 <sup>c</sup>	1.06 <sup>e</sup>
Ga <sup>69</sup>	60.2	3/2	2.0108	.19 <sup>c</sup>	1.28 <sup>e</sup>
As <sup>75</sup>	100.	3/2	1.4349	.29 <sup>d</sup>	1.72 <sup>e</sup>

a. F. Bovey and A. Tiers, NMR Tables (Wiley-Interscience, Inc. New York 1967), 5th ed.

b. The magnitude of coupling constant relating efg to applied electric field is adjusted for the given values of quadrupole moment.

c. G. F. Koster, Phys. Rev. 86, 148 (1952).

d. V. S. Korolkov, A. G. Makhanev, Opt. Spectry. USSR (English Transl.) 12, 87 (1962).

e. D. Gill and N. Bloembergen, Phys. Rev. 129, 2398 (1963).

Figure 3 Arsenic FID's and functional fits using Eq. (19) for samples  
a) MTU (undamaged) and b) MTD600 (quenched from 600°C). In both  
cases the Zeeman field is aligned with the [001] direction. The  
inset shows the indicated portion of the plot with the vertical axis  
enlarged by a factor of 10. In this orientation the FID is not  
affected by damage.

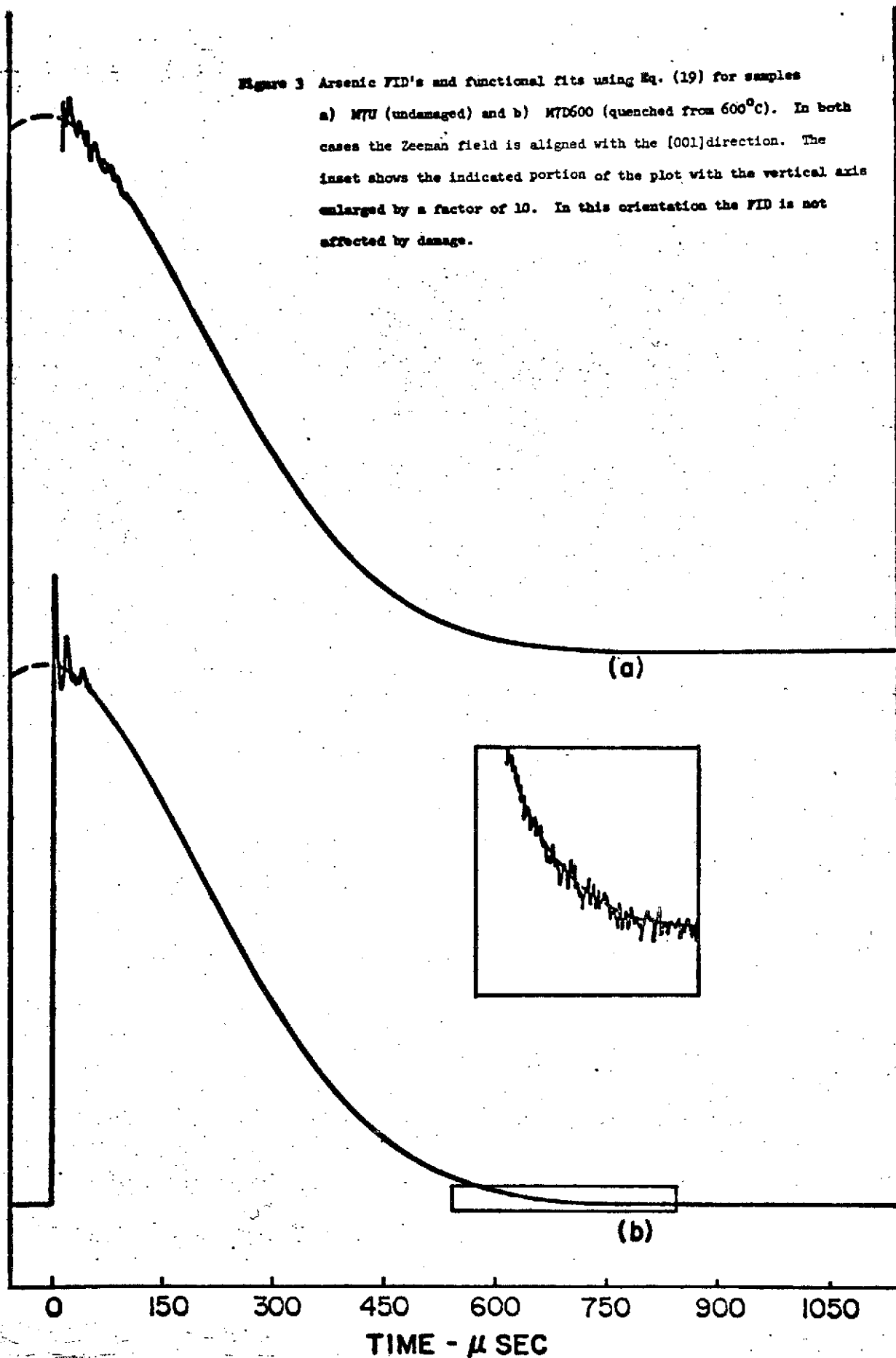
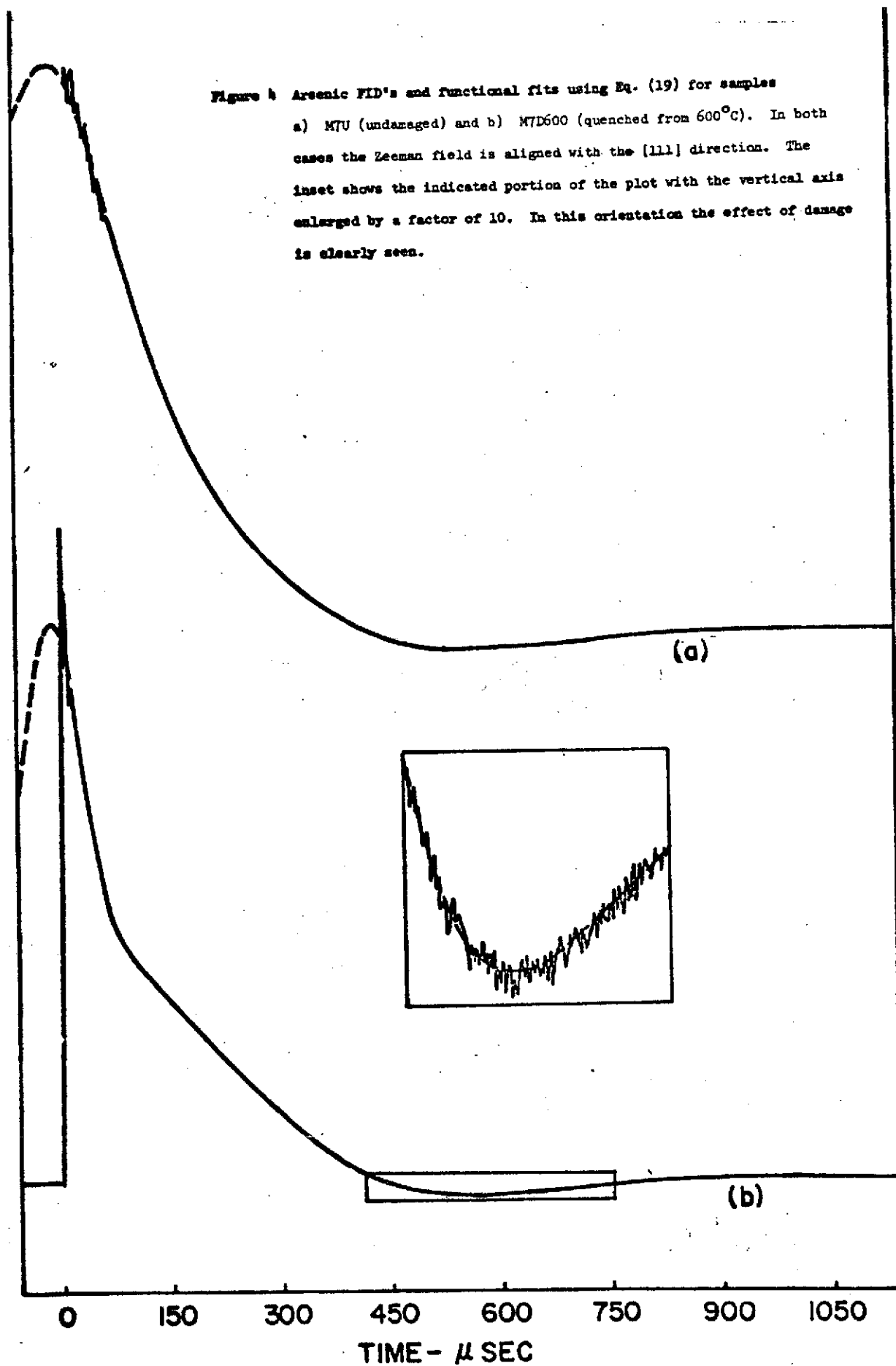


Figure 4 Arsenic FID's and functional fits using Eq. (19) for samples  
a) MTU (undamaged) and b) MTD600 (quenched from 600°C). In both  
cases the Zeeman field is aligned with the [111] direction. The  
inset shows the indicated portion of the plot with the vertical axis  
enlarged by a factor of 10. In this orientation the effect of damage  
is clearly seen.





The Abragam function is successful in describing the FID of a spin  $1/2$  system broadened by the dipolar interaction only. The presence of the like nuclear exchange interaction can alter the shape of the FID substantially without an effect on the second moment<sup>26</sup>. Further, in our lineshape calculation in the Appendix we do not allow the width or shape of the Abragam function to be affected by the quadrupolar interaction. Clearly the presence of a large efg can cause parts of both the like spin dipolar and like spin exchange interactions to become non-secular and may substantially alter the lineshape as well as the second moment.

Certainly part of the deviation of the experimental lineshape from our simplified theory is due to our inability to observe enough of the initial part of the FID so that the fitting routine may determine the parameters accurately. From our theory, the satellite component of the  $\text{As}^{75}$  FID at  $\theta=36^\circ$  in a sample of defect concentration  $10^{16} \text{ cm}^{-3}$  should have a half width of  $23 \mu\text{sec}$ . Thus we can detect only three quarters of the initial intensity of the  $\text{As}^{75}$  FID. Clearly the  $\text{As}^{75}$  data are unreliable in this region of defect concentration for this magnetic field orientation, the [111] direction. In order to measure the broadening in samples of large defect concentration, second moment measurements were made near the  $\theta=\pi/2$  orientation where the initial part of the FID is slow enough to observe accurately. However, even here there are fitting difficulties in samples with large defect concentrations.

As a result of the deviation of the fitting parameters of Eq. (19) from their expected behavior, one can not always interpret these parameters physically

as in the Appendix. However, based on the agreement between the FID and Eq. (19) the second moments are believed accurate. We use only the second moments in the following analysis.

It was shown in Section II that a rotation of the magnetic field about the  $[1\bar{1}0]$  direction results in the second moment varying as

$$\langle \Delta H^2 \rangle = C + D f(\theta). \quad (20)$$

The contributions to the isotropic part C are from the dipolar and exchange mechanisms, while the contributions to D are from the dipolar, pseudodipolar and quadrupolar mechanisms. Parts C and D were determined by fitting the measured second moments at known  $\theta$  to Eq. (20). Generally, sixteen orientations covering a rotation of  $120^\circ$  were used to determine C and D. However, in samples with large defect concentrations only the orientations close to  $\theta = \pi/2$  were used, as few as six orientations. Figs. 5, 6 and 7 show the second moments versus orientation for several samples. Table II contains the coefficients C and D for each isotope in each sample.

Given these isotropic and angular dependent parts, the second moment contributions from the different broadening interactions may be identified. The pure van Vleck dipolar contributions are well known<sup>17</sup>, and they are for each isotope:

$$\langle \Delta H^2 \rangle_D^{71} = .29 + 1.28 f(\theta) \text{ gauss}^2, \quad (21a)$$

$$\langle \Delta H^2 \rangle_D^{69} = .29 + 1.27 f(\theta) \text{ gauss}^2, \quad (21b)$$

$$\langle \Delta H^2 \rangle_D^{75} = .25 + 2.74 f(\theta) \text{ gauss}^2, \quad (21c)$$

where the subscript denotes the broadening mechanism, and the superscript the isotope. NAR data<sup>7</sup> on GaAs yield exchange coupling constants. Including only nearest and next nearest neighbor interactions, the unlike exchange contributions

TABLE II. MEASURED SECOND MOMENTS AS A FUNCTION OF  
MAGNETIC FIELD ORIENTATION. THE SECOND MOMENT  
IS EXPRESSED AS  $C + D \cos^2 \theta$  IN UNITS OF GAUSS<sup>2</sup>

Sample <sup>a</sup>	Ga <sup>71</sup>		Ga <sup>69</sup>		As <sup>75</sup>	
	C	D	C	D	C	D
M7U	.58±.02	.68±.06	.64±.03	1.18±.08	1.44±.07	4.73±.36
M2U	.64±.03	.63±.07	.64±.03	1.22±.10	1.32±.07	5.58±.66
M3U	.65±.04	.69±.10	.72±.03	1.30±.11	1.37±.01	4.63±.04
M7D500	.58±.03	.77±.08	.63±.01	1.79±.02	1.40±.10	7.30±.85
M2D550	.64±.03	1.30±.10	.66±.04	3.92±.19	1.23±.08	17.2±1.23
M3D600	.69±.01	1.84±.03	.72±.04	5.05±.51	1.15±.08	19.4±1.60
M7D600	.63±.04	1.98±.13	.72±.04	6.08±.45	1.30±.14	24.9±1.61
M5D700	.65±.04	2.40±.23	.88±.07	7.46±.58	1.66±.14	21.2±1.14
EMC(Si)	.72±.05	3.18±.29	.95±.08	7.34±.73	2.83±.23	25.1±2.34

- a) Sample identification M2D500 means a Monsanto crystal quenched from 500°C.  
Undamaged samples are labeled with a U. EMC(Si) is a Si doped sample purchased from Electronic Materials Corp. with a carrier concentration of  $4 \times 10^{16} \text{ cm}^{-3}$ .

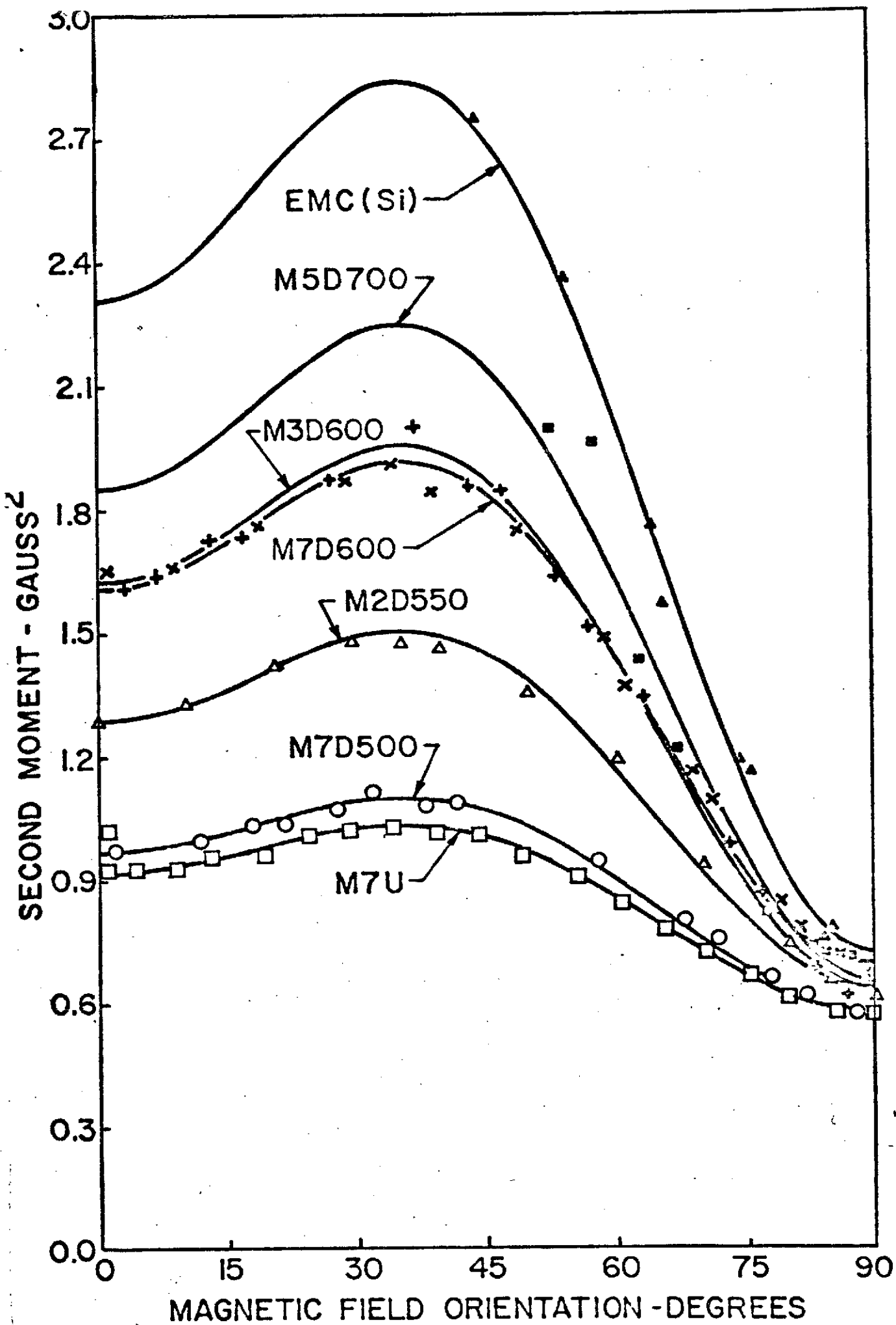


Figure 5  $\text{Ga}^{71}$  second moments as a function of magnetic field orientation for some samples in Table II. The solid lines are the best fits using Eq. (20). Only representative data points are shown.

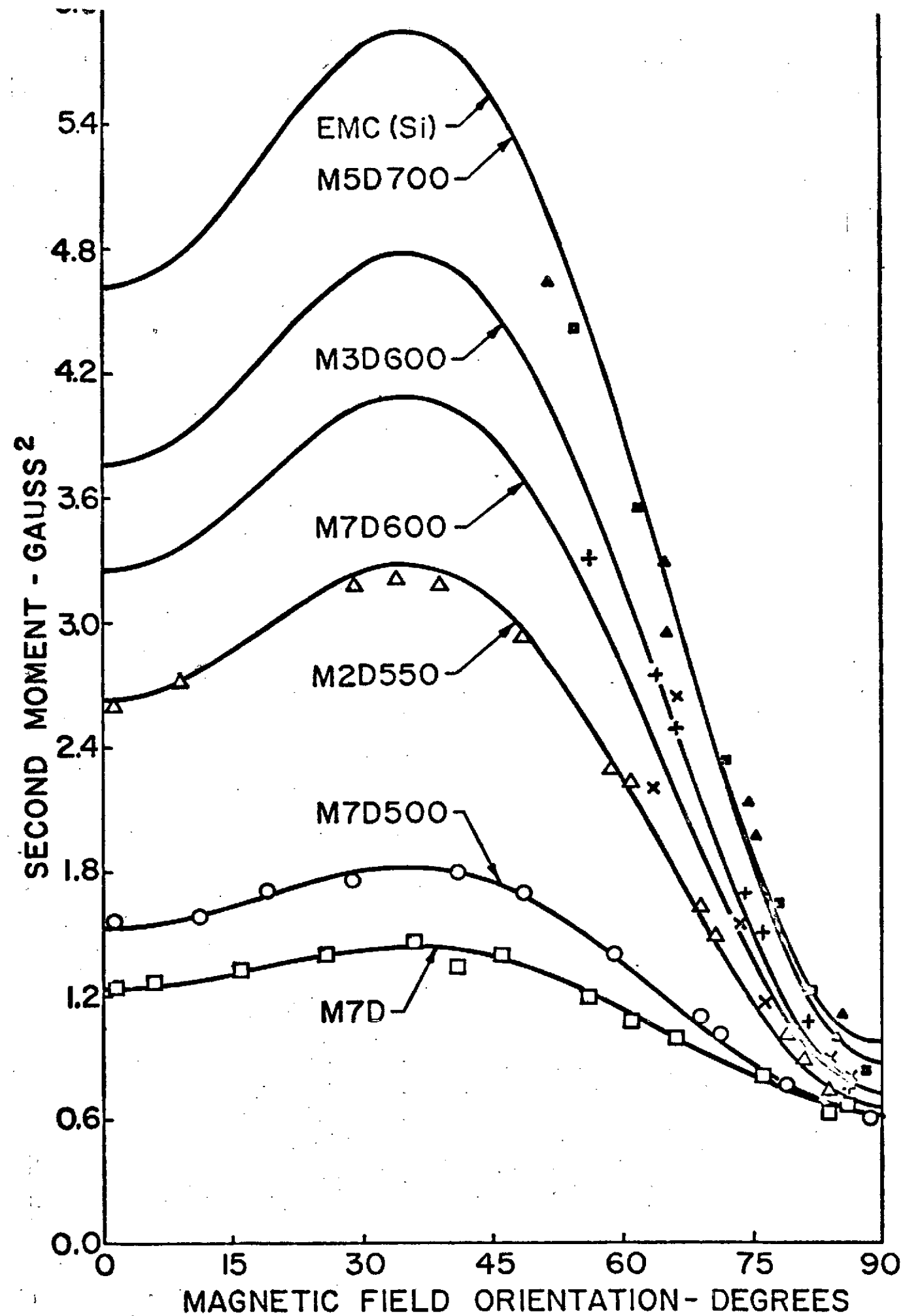


Figure 6  $^{69}\text{Ga}$  second moments as a function of magnetic field orientation for some samples in Table II. The solid lines are the best fits using Eq. (20). Only representative data points are shown. The curves for EMC(Si) and M5D700 coincide.

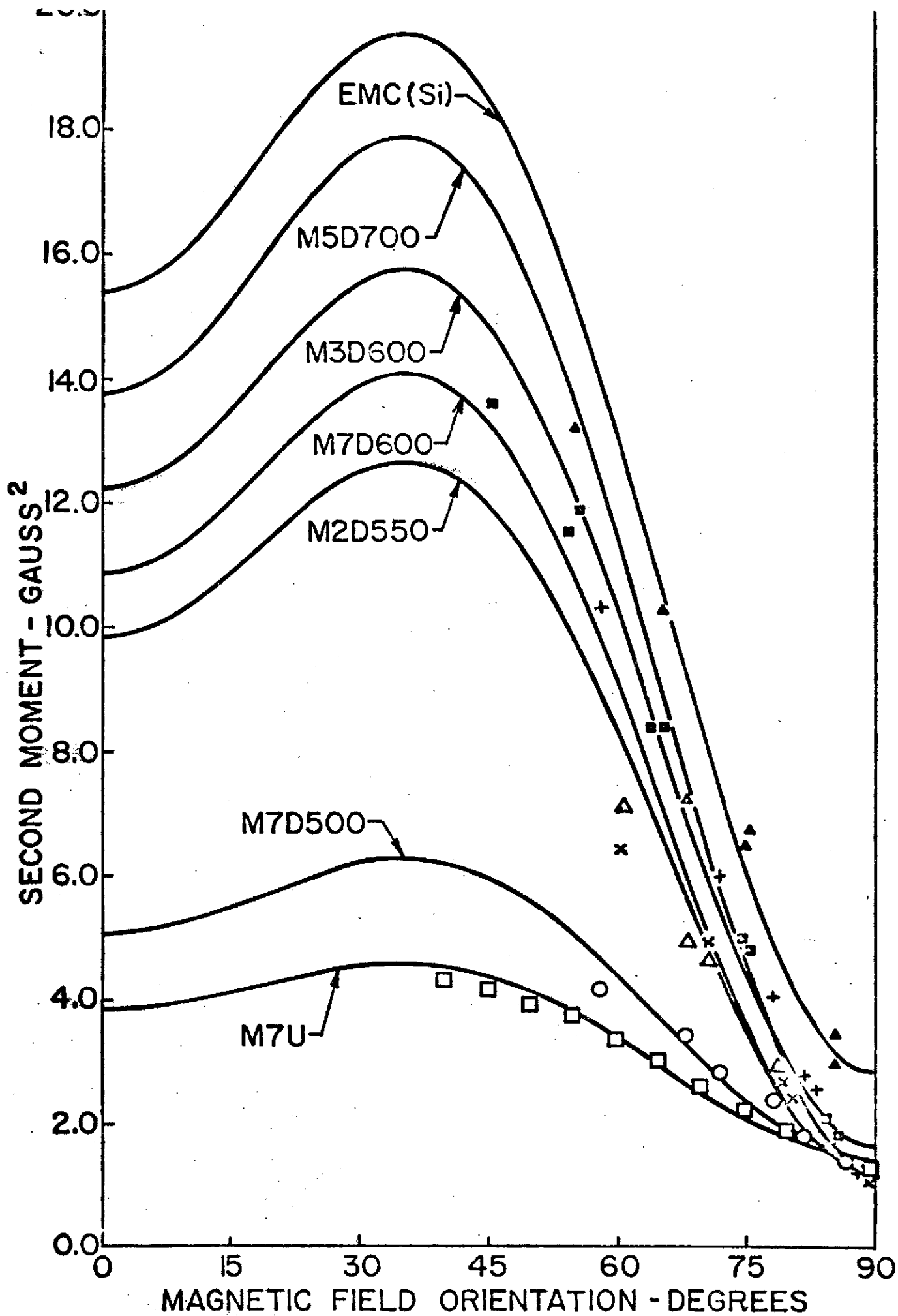


Figure 7  $A_{75}$  second moments as a function of magnetic field orientation for some samples in Table II. The solid lines are the best fits using Eq. (20). Only representative data points are shown.

to the second moments are

$$\langle \Delta H^2 \rangle_E^{71} = .25 \text{ gauss}^2, \quad (22a)$$

$$\langle \Delta H^2 \rangle_E^{69} = .24 \text{ gauss}^2, \quad (22b)$$

$$\langle \Delta H^2 \rangle_E^{75} = .58 \text{ gauss}^2. \quad (22c)$$

Subtracting the contributions (21) and (22) from our data leaves only the contributions from the quadrupolar and pseudodipolar interactions. Our analysis predicts that these contributions will have no isotropic part, and, as can be seen from Table II and Eqs. (21) and (22), the isotropic remainder is negligibly small for the two Ga isotopes. In samples of large quadrupolar broadening, however, the isotropic remainder is larger than predicted on the basis of dipolar and exchange contributions.

In order to separate the contributions from the quadrupolar and pseudodipolar interactions we use the fact that the pseudodipolar broadening in  $\text{gauss}^2$  is the same for both Ga isotopes. This is because only the four nearest neighbors, all As nuclei, contribute significantly to the pseudodipolar broadening. Then the difference in the remaining angular parts of the Ga second moments must be due to quadrupolar broadening. Both Ga isotopes experience the same random efg, so the difference in their quadrupolar contributions must be due to the difference in their nuclear properties. Since  $\langle \Delta H^2 \rangle_Q \propto Q_I^2 / \delta_I^2$ , we may write that

$$\langle \Delta H^2 \rangle_Q^{69} = K \langle \Delta H^2 \rangle_Q^{71} \quad (23)$$

where  $K = (Q_{69} \delta_{71} / Q_{71} \delta_{69})^2$ .

If  $D_R^{71}$  and  $D_R^{69}$  are the remaining angular parts of the  $\text{Ga}^{71}$  and  $\text{Ga}^{69}$  second moments,

respectively; then

$$\langle \Delta H^2 \rangle_Q^{71} = (K-1)^{-1} (D_R^{69} - D_R^{71}). \quad (24)$$

The relevant nuclear properties are shown in Table I. The values of  $R_{14}$  have been adjusted for more recent values of electric quadrupole moment. Gill and Bloembergen give different numbers for the values of  $R_{14}$  for the two Ga isotopes. Physically we see no grounds for this difference, and thus a weighted average value of  $1.2 \times 10^{10} \text{ cm}^{-1}$  is used for both. The  $\text{Ga}^{69}$  value is weighted heavier because the experiment on  $\text{Ga}^{69}$  was probably more accurate, due to the better S/N and greater quadrupole shift than  $\text{Ga}^{71}$ . Another experimental measurement of  $R_{14}$  has been performed<sup>14</sup>. In this experiment  $R_{14}$  was measured dynamically by observing the nuclear transitions caused by an rf electric field. The evaluation of  $R_{14}$  involves more manipulation than the straightforward experiment of Gill and Bloembergen. For this reason the static measurements of  $R_{14}$  are used here.

Once  $\langle \Delta H^2 \rangle_Q^{71}$  and  $\langle \Delta H^2 \rangle_Q^{69}$  have been established we may find the Ga pseudodipolar contribution

$$\langle \Delta H^2 \rangle_P^{71} = \langle \Delta H^2 \rangle_P^{69} = (K-1)^{-1} (K D_R^{71} - D_R^{69}). \quad (25)$$

Comparing Eqs. (25) and (9), we obtain an a quadratic expression for the pseudodipolar coupling constant  $\tilde{B}_{NN}$  in terms of  $D_R^{71}$  and  $D_R^{69}$ . There are two solutions for  $\tilde{B}_{NN}$ , and this experiment cannot distinguish between them. In the case of GaAs both solutions are negative in sign.

The pseudodipolar interaction is proportional to the magnetic dipole moments of the interacting nuclei<sup>5</sup>. Thus we may write

$$\langle \Delta H^2 \rangle_P^{75} = (.4\gamma_{71}^2 + .6\gamma_{69}^2) \gamma_{75}^{-2} \langle \Delta H^2 \rangle_P^{71}, \quad (26)$$



where .4 and .6 are the relative abundances of  $\text{Ga}^{71}$  and  $\text{Ga}^{69}$ , respectively. The quadrupolar second moment contribution is just the remaining angular part,  $D_R^{75}$ , less the pseudodipolar contribution  $\langle \Delta H^2 \rangle_P^{75}$ . With the quadrupolar contributions to the second moments determined, we may calculate the concentration of charged defects. For nuclear spin  $I = 3/2$ , Eq. (16) reduces to

$$\langle \Delta H^2 \rangle_Q = \frac{1}{10} \left( \frac{e e^* R_{14} Q_I}{\epsilon \gamma_I h} \right)^2 \left( \frac{\rho_I}{\rho} \right) f(\theta) \sum_j r_j^{-4}. \quad (27)$$

The defect density  $\rho_I$  is found from Eq. (27) by identifying  $\langle \Delta H^2 \rangle_Q$  with the measured quadrupolar second moment. Table III contains the quadrupolar second moments, the pseudodipolar coupling constant, and the charged defect densities for each sample.

Agreement of the defect densities as measured by Ga and As resonances is obtained only if we assume that the defects are preferentially located on the As sublattice. When this is true, the As nuclei are generally further from a defect than the Ga nuclei and will experience a smaller quadrupolar interaction. Thus the value of the lattice sum in Eqs. (16) or (27) depends upon which sublattice contains the defects. The defect densities listed in Table III are calculated assuming As monovacancies.

Another assumption in the calculation of the defect densities of Table III is that the effective charge of a defect is the electronic charge, or  $e^* = e$ . We assume a model in which the GaAs lattice is mostly covalently bonded, but retains some ionic character. The calculation of Harrison<sup>27</sup> yields a net charge of  $+0.87e$  on the Ga site and a net charge of  $-0.87e$  on the As site, where the electron

TABLE III. QUADRUPOLEAR SECOND MOMENTS, DEFECT DENSITIES, AND PSEUDODIPOLAR COUPLING CONSTANTS. DEFECT DENSITIES ASSUME AN ARSENIC MONOVACANCY OF CHARGE  $e$ .

Sample	$\langle \Delta H^2 \rangle_\phi$ (gauss <sup>2</sup> )			Defect Density ( $10^{15} \text{ cm}^{-3}$ )		Pseudodipolar Coupling Constant $B_{NN}$
	Ga <sup>71</sup>	Ga <sup>69</sup>	As <sup>75</sup>	As Measured By Ga	As	
M7U	.17±.03	.67±.13	3.85±.41	.21±.04	.24±.03	-1.54, -.46±.05
M2U	.18±.04	.73±.16	4.75±.70	.22±.05	.30±.05	-1.52, -.48±.06
M3U	.20±.05	.81±.20	3.83±.34	.20±.06	.23±.02	-1.53, -.47±.08
M7D500	.34±.03	1.36±.11	6.62±.89	.42±.04	.42±.06	-1.47, -.53±.06
M2D550	.86±.07	3.48±.28	16.6±1.28	1.07±.09	1.04±.08	-1.48, -.52±.09
M3D600	1.12±.17	4.51±.68	18.5±1.66	1.39±.21	1.16±.11	-1.57, -.43±.08
M7D600	1.33±.15	5.36±.62	23.7±1.70	1.65±.20	1.49±.11	-1.65, -.35±.12
M5D700	1.67±.26	6.73±1.04	19.8±1.44	2.07±.32	1.25±.10	-1.70, -.30±.18

has charge  $-e$ . If we remove a neutral As atom from the lattice and allow electronic charge shifts on only the four nearest neighbors, then each neighboring Ga ion acquires a net charge of  $0.55e$ . Now there will be a certain ionization energy for these four neighboring Ga ions to collectively give up one electron to the conduction band and in the process acquire an additional  $.25e$  charge each. Then each Ga ion has a charge  $0.9e$ , very nearly the  $0.87e$  each had before the vacancy was produced. This small change in effective charge implies a small change in the bonding orbitals. On this basis we expect that the activation energy for ionization is small. The induced efg is sensitive to the change in the charge distribution. This difference is just  $0.87e$  localized at the site of the As vacancy and  $+0.03e$  at each neighboring Ga site. This appears very much like a point charge defect to all nuclei, even the nearest Ga neighbors.

## V. DISCUSSION

### a) Pseudodipolar Interaction

The presence of the pseudodipolar interaction in III-V compounds has been recognized only recently<sup>8</sup>. One reason for this is that the nuclei in these compounds generally experience quadrupole interactions ( $P^{31}$  is the only exception). Since the magnetic field orientation dependence of the second moment contributions from each interaction has the form  $C + Df(\theta)$ , the quadrupolar broadening can easily mask the effect of the pseudodipolar interaction. There would have been no clear evidence of the pseudodipolar interaction in this experiment had not our crystals been good enough so that the second moments of the Ga resonances were smaller than those calculated from the dipolar interaction alone. We now expect that the pseudodipolar interaction will be found in all III-V compounds.

There have been several theoretical treatments of electron coupled interactions, both from a band structure approach<sup>4-6</sup> and using localized bonding models.<sup>13,28,29</sup> In order to calculate the coupling constants from band theory, greatly simplified band structures were used. These calculations are very coarse. The localized bonding model calculations predict the negative sign of  $\tilde{B}_{ij}$  observed in  $TlCl$ <sup>13</sup>,  $InP$ <sup>8</sup>, and now in  $GaAs$ . However, these calculations do not agree quantitatively with our data or the  $InP$  data.

In the treatment by Clough and Goldberg<sup>13</sup>, it was noted that while

the absolute magnitude of  $\tilde{B}_{ij}$  and  $\tilde{A}_{ij}$  depend upon the degree of covalency  $\lambda$  of the bond, the ratio  $|\tilde{B}_{ij}/\tilde{A}_{ij}|$  is independent of  $\lambda$ . In their model they find that this ratio has a maximum value of 1/2 for purely p orbitals. Larger values have been measured in III-V compounds. Englesberg and Norberg<sup>8</sup> observed a  $|\tilde{B}_{ij}/\tilde{A}_{ij}|$  ratio of 1.8 in a single crystal of InP and 1.5 in a powder sample. We measure a value of .73 or 2.2 in a single crystals of GaAs, depending upon which solution of Eq. (9) is physical.

Clough and Goldburg developed their expressions for TlCl crystals. One should not expect that the same model can accurately describe III-V compounds. Their method begins by assuming a fixed degree of covalent character to the bonds. This covalent part of the bond is then represented by a variable admixture of s and p orbitals on each of the atoms contributing to the bond. They then find, using second order perturbation theory, an expression for the  $|\tilde{B}_{ij}/\tilde{A}_{ij}|$  ratio as a function of the amount of s and p character in the bond.

The application of their model to GaAs has two major defects. It does not account for the d state admixtures in the wave functions that are known to be important. The second problem is that in polar semiconductors the wave function of valence electrons moves toward the anion<sup>27</sup>(As), while the wave function for the conduction band shifts toward the cation<sup>30</sup>(Ga). Since the exchange and pseudodipolar interactions are related to the overlap of the valence and conduction band wave functions, a model like Clough and Goldburg's, that assumes a fixed covalent character to the bond for both the valence and conduction bands, will miss the consequences of the wave function shift between the cation and the anion. A modification of their calculation that accounts for the relative displacements of valence and conduction electron wave functions and the d state admixtures should

be more accurate.

#### b.) Quadrupolar Effects

An independent method of estimating the defect concentration is desirable, and the experimental data of Potts and Pearson enable one such determination. Their minimum quenching temperature was  $1000^{\circ}\text{C}$ , generating a defect density of  $\sim 2 \times 10^{18} \text{ cm}^{-3}$ . Thus we must extrapolate over three orders of magnitude to compare with the defect density expected following a quench from a temperature in the  $500^{\circ}\text{C}$  to  $700^{\circ}\text{C}$  range. In Fig. 8 the log of the defect density is plotted against the reciprocal quenching temperature,  $T_q^{-1}$ . The measurements of Potts and Pearson are shown, as well as the dashed line showing the extrapolation based on their entropy and enthalpy values for the formation of a vacancy.

It is clear that our observed concentrations are greater than those projected. However, Potts and Pearson expressed some uncertainty in the proportionality constant relating the rms deviation in lattice parameter and the concentration of monovacancies. This puts the accuracy of their measured vacancy concentrations in doubt by a multiplicative constant. Further, the reliability of an extrapolation over three orders of magnitude is questionable. In Fig. 8 it can be seen that a small error in the activation energy found at a defect concentration of  $10^{19} \text{ cm}^{-3}$  makes a substantial difference when extrapolated to  $10^{15} \text{ cm}^{-3}$ . In addition, there is no a priori reason to believe that the same physical mechanism is dominant over the entire temperature range.

We believe that the As vacancies are caused by the As atoms lost to the equilibrium vapor phase during the heating process. The equilibrium  $\text{As}_2$  and  $\text{As}_4$  vapor pressures are known<sup>31</sup> as a function of temperature in the  $675^{\circ}\text{C}$  to  $925^{\circ}\text{C}$

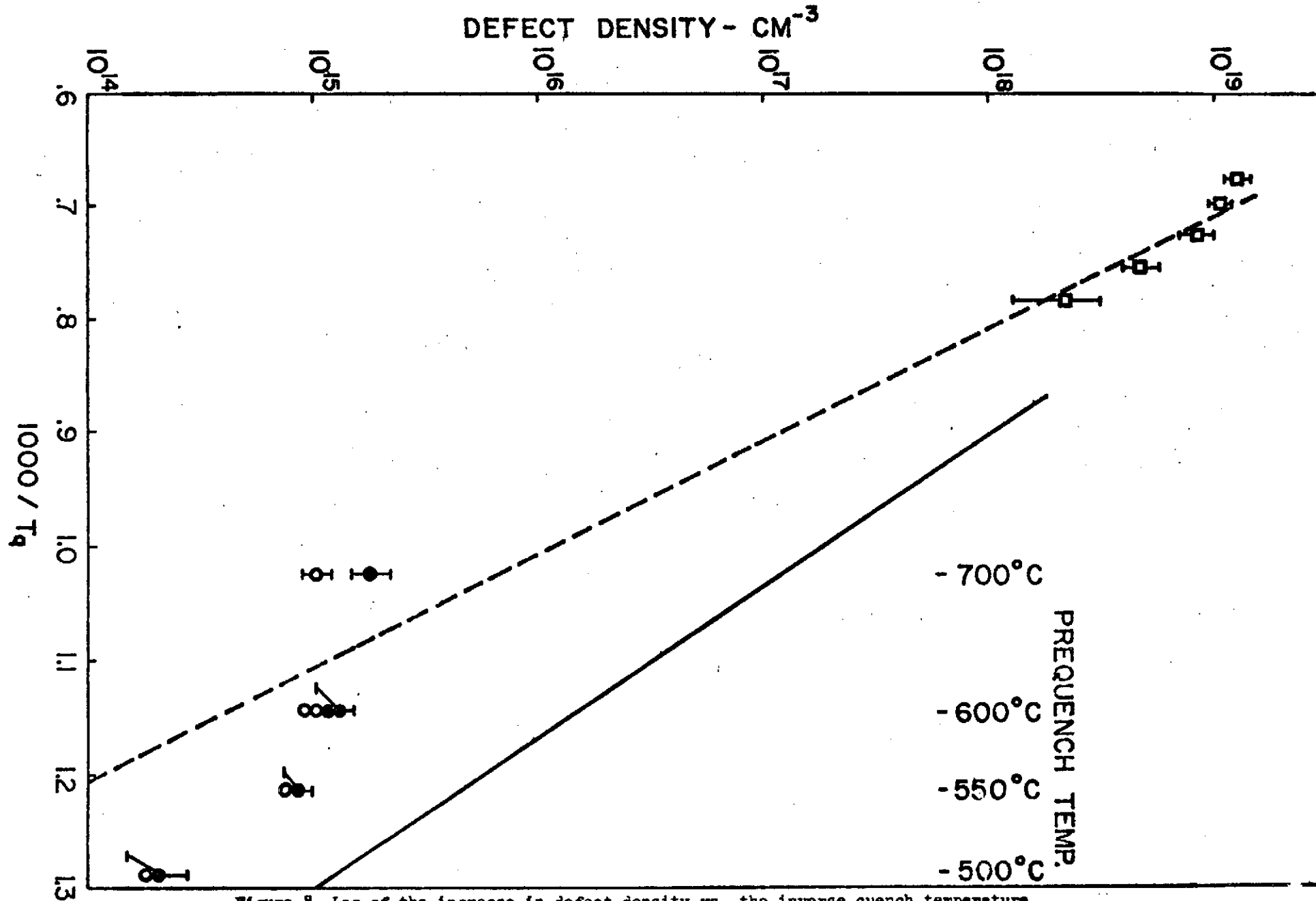


Figure 8 Log of the increase in defect density vs. the inverse quench temperature.

Also shown are the defect measurements of Potts and Pearson. The dashed line is an extrapolation of their measurements to smaller defect densities. The solid line shows our calculation of defect densities using vapor pressure data. The error bars shown are typical of that temperature.

range. Thus we can calculate the number of As atoms removed from a sample heated in an initially evacuated tube of a given size. The ratio of this number to the sample volume is the concentration of As monovacancies produced by this process. This calculation is shown in Fig. 8 as the solid line. Using the condition that each defect of charge  $e$  is located on the As sublattice, and using the low frequency dielectric constant for  $\epsilon$ , our observed defect concentrations are smaller than the vapor pressure calculation. This calculation is meant for order of magnitude comparison, and it assumes that the ratio of tube to sample volumes was 10 for all samples. Generally, our tube volumes were larger, so the solid line in Fig. 8 should represent the minimum number of defects produced.<sup>32</sup>

If the sample behaves as an infinite source of As vapor, supplying whatever is necessary to reach equilibrium at a given temperature, then the defect density present following a quench depends additively upon that prior to the quench. In order to determine the temperature dependence the defect density in each sample prior to the quench must be subtracted from the measured density following the quench. Our data in Fig. 8 have been adjusted to account for prequench defect densities.

The slope of our lowest temperature data is in agreement, within experimental error, with the vapor pressure activation energy. Using the two most reliable temperatures, 500°C and 550°C, we measure an activation energy of  $1.5 \pm 0.1$  eV. The activation energy reported by Potts and Pearson is 2.0 eV, and the vapor pressure data yield 1.4 eV.

There are several possible explanations for the fact that our measurements of defect concentrations are smaller than those calculated from vapor



pressure data. One is the dependence on the experimental value of the product  $R_{14}^2 Q^2$ . A small error in the values of  $R_{14}$  or  $Q$  can make a substantial error in our analysis of the defect densities. The error bars shown in Fig. 8 do not account for errors in these quantities.

Another explanation is that the thermal damage did not produce as many vacancies as predicted. This could have occurred in two ways: 1) the sample was not in thermal equilibrium with the vapor, so the vapor phase did not consist of as many As molecules as predicted; or 2) the vapor pressure data are wrong. Using self diffusion data<sup>19</sup> it is estimated that the sample will reach thermal equilibrium in approximately 10 hours, and also it is unlikely that the As vapor can re-enter the lattice during the quench. Further, the vapor pressure data accuracy is well established by several workers,<sup>31</sup> so we have confidence in the number of As atoms in the equilibrium vapor phase. It is concluded that at least as many vacancies were produced as predicted by the vapor pressure data.

This experiment measures the charged defect concentration. The effect of the strain caused by an uncharged impurity is not sufficiently strong to be noticed when charged defects are also present. Another possible explanation of our apparently low defect concentrations is that not every As vacancy acquires a charge of magnitude  $e$ . This can happen in two ways. One is that each As vacancy assumes an effective charge  $e^*$  such that  $e^* < e$ . However, we have already shown that the model in which  $e^* \approx e$  discussed in Section IV is reasonable. The other is that the activation energy for ionization of the defect is such that at room temperature not all the impurities are charged. An experiment investigating the temperature dependence of the NMR second moment is expected to check this latter possibility.

Our analysis uses the induced quadrupolar interaction, and the efg associated with a charged defect decreases as  $r^{-2}$  because we have assumed that the defect appears as a point charge. However, electronic screening or defect complexes may exist, causing the efg to decrease faster than  $r^{-2}$ . We have calculated the Debye-Hückel screening length for the Monsanto sample and find it to be negligible, so screening by free electrons is not important. Defect complexes can, however, make a substantial effect. For example, an As vacancy may pair with an acceptor to produce a localized electric dipole moment. In this case the efg will decrease as  $r^{-3}$ , the effective broadening range of the defect will be reduced, and many more impurities will be necessary to produce a given quadrupole contribution to the second moment. A double resonance experiment detecting nearest nuclei of the impurity as the rare spins will address the question of defect complexes.

#### c) Experimental Limitation

It is possible that the low values of defect concentration measured in samples quenched at 600°C and 700°C are accurate. This effect could be caused by vacancy clustering or vacancy-acceptor pairing. However, it is more likely that these low values are due to the current limitations in our experiment and analysis. There are several trends in the data that indicate that the present measurement of defect density errs if concentrations are larger than  $\sim 10^{15} \text{ cm}^{-3}$ . One trend, discussed in Section IV, is the observed deviation of the FID functional fitting parameters in Eq. (19) from physically interpretable quantities. This deviation is always present in the As<sup>75</sup> and Ga<sup>69</sup> data. It appears in the Ga<sup>71</sup> data

for samples quenched from 600°C and higher. We also find that the increases in the second moment caused by thermal damage at 600°C and 700°C are proportionately smaller for nuclei with larger quadrupole moments. That is, the ratios of the increase in the  $\text{Ga}^{71}$  second moment to the increase in the  $\text{Ga}^{69}$  and  $\text{As}^{75}$  second moments are greater than expected. These ratios should be fixed by the nuclear properties. It is clear that the fast component of the FID decays so quickly in the presence of these large quadrupole interactions that our fitting analysis is not sensitive enough to it. With our analysis this results in a deviation in the pseudodipolar coupling constant and a disagreement between the defect densities as measured by Ga and As resonances.

Additional evidence that this experiment cannot measure relatively large defect concentrations is seen in the data for the Si doped sample. The  $\text{Ga}^{69}$  second moments are much smaller than one expects from the large second moments of  $\text{Ga}^{71}$ . To an even greater extent, the same is true of  $\text{As}^{75}$ . Assuming that the pseudodipolar interaction is the same in all GaAs crystals, and assuming that the ionized Si donors are located on Ga sites, then the  $\text{Ga}^{71}$  data indicate a charged defect density of  $6.4 \times 10^{15} \text{ cm}^{-3}$ , where we have accounted for the Debye-Hückel screening. Hall effect measurements yield a carrier concentration of  $4 \times 10^{16} \text{ cm}^{-3}$ , so there are at least that many ionized impurities. With our current experimental limitations, this technique is too sensitive to accurately measure charged defect concentrations greater than  $10^{15} \text{ cm}^{-3}$ .

We conclude that our present experiment does not dependably measure frequency second moments larger than  $5 \text{ kHz}^2$ . This corresponds to a FID half width of approximately 70  $\mu\text{sec}$ . In the  $\text{Ga}^{71}$ ,  $\text{Ga}^{69}$ , and  $\text{As}^{75}$  resonances this corresponds

to charged defect densities of  $2.5 \times 10^{15} \text{ cm}^{-3}$ ,  $9 \times 10^{14} \text{ cm}^{-3}$ , and  $2 \times 10^{14} \text{ cm}^{-3}$ , respectively. In order to make equivalent cw measurements, excellent S/N is required at least as far as 5 kHz from the center frequency. With improved damping of the piezoelectric noise and with spin locking techniques we expect these upper limits to be extended to charged defect densities near  $10^{17} \text{ cm}^{-3}$ . At these concentrations we expect that second order quadrupolar effects will be important, and that the lineshape will have changed substantially.

The lower limit of measurable charged defect concentration would occur where the quadrupole contribution to the As second moment is just measureable, say  $0.1 \text{ gauss}^2$ . This corresponds to a defect density of  $6 \times 10^{12} \text{ cm}^{-3}$  on the As sublattice or  $3 \times 10^{12} \text{ cm}^{-3}$  on the Ga sublattice, representing a defect to atom ratio of the order of  $10^{-10}$ . When this method is applicable, it rivals the sensitivity of neutron activation measurements, and in addition, the NMR method can observe vacancies.

In summary, while questions remain about the effective charge and the volume dependence of the defect densities, it is clear that the NMR lines in GaAs are extremely sensitive to impurity concentrations. In fact, they are so sensitive that in samples of carrier concentration of  $10^{16} \text{ cm}^{-3}$  this first order line shape and second moment analysis is insufficient to treat the problem. Using this undoped semi-insulating single crystal, we have observed a negative coupling constant for the pseudodipolar interaction and developed a method by which the pseudodipolar, dipolar, and quadrupolar second moment contributions can be identified. We have made two estimates of the defect concentrations produced by thermal quenching, using independent sets of experimental data. Our measurements

lie between these two calculations, above the Potts and Pearson projection and below the vapor pressure estimate. That our method of analysis is correct is adequately demonstrated by two facts. One is that the pseudodipolar interaction, within experimental error, remains independent of the total second moment, i.e. thermal damage. The second is that the charged defect densities as measured by Ga and by As resonances agree for samples with small concentrations.

## VI. ACKNOWLEDGEMENTS

We wish to thank I. J. Lowe for helpful conversations, R. K. Cueman, J. W. Kaufer and P. A. Millington for assistance during the experiment, and L. H. Botten for equipment design and construction.

## APPENDIX

The objective of this appendix is to compute the NMR line shape due to the quadrupolar interaction using a continuum crystal model. From Eqs. (3g), (12) and (13) the satellite frequency shift of a spin 3/2 nucleus located a distance  $\underline{r}$  from a charged impurity is

$$\Delta\nu = -\underline{\alpha} \cdot \underline{r} / r^3, \quad (\text{A1})$$

where

$$\underline{\alpha} = \frac{ee^*QR_{14}}{\epsilon h} \left( n_y n_z \hat{x} + n_x n_z \hat{y} + n_x n_y \hat{z} \right). \quad (\text{A2})$$

We calculate the volume  $\Omega$  about a single impurity containing nuclei with frequency shifts greater than some  $\Delta\nu$ .

The volume  $\Omega$  is bounded by a revolution about the  $\underline{\alpha}$  direction of a curve described by

$$r^2 = -\alpha \cos\phi / \Delta\nu, \quad (\text{A3})$$

where  $\phi$  is the angle between  $\underline{r}$  and  $\underline{\alpha}$ . For  $\phi=0$  there is a minimum frequency shift  $\Delta\nu_0 = \alpha/r_0^2$  for the nuclei located on the crystal surface, a distance  $r_0$  from the impurity. The maximum frequency shift is  $\Delta\nu_m = \alpha/\alpha^2$ , for the nearest neighbor nuclei located at a distance  $\underline{a}$  from the impurity. The volume within the

nearest neighbor sites and outside the sample are excluded from  $\Omega$ . These exclusions eliminate unphysical infinities. The line shape will be shown to be independent of  $r_0$  but not of  $a$ . Thus the sample dimension  $r_0$  has no effect upon the line shape. Further, the near neighbor distance  $a$  may be used to determine the location of the defect sites. The volume  $\Omega$  is found by a simple integration, and the result is

$$\Omega(\Delta\nu) = \frac{4\pi}{3} \begin{cases} r_0^3 \left(1 - \frac{3}{5} \Delta\nu/\Delta\nu_0\right) - a^3 \left(1 - \frac{3}{5} \Delta\nu/\Delta\nu_m\right), & \Delta\nu \leq \Delta\nu_0 \\ \frac{2}{5} (a/\Delta\nu)^{3/2} - a^3 \left(1 - \frac{3}{5} \Delta\nu/\Delta\nu_m\right), & \Delta\nu_0 \leq \Delta\nu \leq \Delta\nu_m \\ 0, & \Delta\nu_m < \Delta\nu \end{cases} \quad (A4)$$

The number of nuclei  $N_s(\Delta\nu)$  shifted by an amount greater than  $\Delta\nu$  is  $(3N/4\pi r_0^3)\Omega(\Delta\nu)$ , where  $N$  is the number of resonant nuclei in the sample. Then the distribution  $g(\Delta\nu)$  of frequency shifts caused by a single impurity is

$$g(\Delta\nu) = - \frac{dN_s}{d\Delta\nu} \quad (A5)$$

Combining Eqs. (A4) and (A5) the expression for  $g(\Delta\nu)$  becomes

$$g(\Delta\nu) = \frac{3N}{5\Delta\nu_0} \begin{cases} 1 - (\Delta\nu_0/\Delta\nu_m)^{5/2}, & \Delta\nu < \Delta\nu_0 \\ (\Delta\nu_0/\Delta\nu)^{5/2} - (\Delta\nu_0/\Delta\nu_m)^{5/2}, & \Delta\nu_0 \leq \Delta\nu \leq \Delta\nu_m \\ 0, & \Delta\nu_m < \Delta\nu \end{cases} \quad (A6)$$



Next the frequency shift distribution due to a number  $N_I$  of impurities randomly distributed throughout the sample must be calculated. Due to the long range nature of the induced efg, the satellite transitions of each nucleus are significantly affected by many defects, even at very low defect concentrations ( $10^{12} \text{ cm}^{-3}$ ). Thus one may use the central limits theorem to calculate the frequency shift distribution due to a number  $N_I$  of randomly distributed defects. According to that theorem, the distribution will be gaussian with a second moment given by

$$\langle \Delta \nu^2 \rangle_Q = N_I \langle \Delta \nu_1^2 \rangle_Q,$$

where  $\langle \Delta \nu_1^2 \rangle_Q$  is the second moment of  $g(\Delta \nu)$ . Using the relation  $\Delta \nu_0 / \Delta \nu_m = a/r \ll 1$ , one finds

$$\langle \Delta \nu^2 \rangle_Q = \frac{2\pi e^2 e^{*2} Q^2 R_{14}^2}{3 a h^2 \epsilon^2} \rho_I f(\theta), \quad (\text{A7})$$

where  $\theta$  is defined in Eq. (7), and  $\rho_I$  is the charged defect density.<sup>33</sup>

Finally, the relation between the distribution of quadrupole frequency shifts  $G_Q(\Delta \nu)$  (basically an inhomogeneous broadening), and the NMR line shape  $G(\nu)$  must be established. The quadrupole frequency shift distribution is a gaussian function with second moment  $\langle \Delta \nu^2 \rangle_Q$ :

$$G_Q(\Delta \nu) = (2\pi \langle \Delta \nu^2 \rangle_Q)^{-\frac{1}{2}} \exp(-\Delta \nu^2 / 2 \langle \Delta \nu^2 \rangle_Q). \quad (\text{A8})$$

For the spin 3/2 case, the magnetic resonance line shape is found through the expression

$$G(\nu) = \int_{-\infty}^{\infty} d(\Delta \nu) G_Q(\Delta \nu) \left[ .3 G_{\frac{1}{2}, \frac{3}{2}}(\nu - \Delta \nu, \Delta \nu) + .4 G_{\frac{3}{2}, \frac{1}{2}}(\nu, \Delta \nu) + .3 G_{\frac{3}{2}, -\frac{1}{2}}(\nu + \Delta \nu, \Delta \nu) \right], \quad (\text{A9})$$

where  $G_{1/2, 3/2}(\nu - \Delta \nu, \Delta \nu)$  is the line shape function of the 3/2-1/2 transition caused by other broadening mechanisms (as modified by the quadrupole shifts). The

first argument in the functional dependence of  $G_{1/2,3/2}$  is the center frequency for the 1/2-3/2 transition, and the second is intended to represent the effect the shift may cause on the line shape. The shape due to other interactions can be modified by the shifts, e.g. terms in the dipolar hamiltonian that are secular in the absence of shifts will become non-secular when the shifts are large enough, thus modifying the width of the dipolar broadened line.  $G_{-1/2,1/2}$  and  $G_{-3/2,-1/2}$  are the corresponding shape functions for those transitions. The factors 0.3, 0.4, and 0.3 are weighting factors that arise from the transition matrix elements for the three transitions.

For the case of low defect concentrations treated here, we ignore the effect of the frequency shift upon the line shape. Further we assume that  $G_{1/2,3/2}(\nu, 0) = G_{-1/2,1/2}(\nu, 0) = G_{-3/2,-1/2}(\nu, 0) = G_0(\nu)$  where  $G_0(\nu)$  is the lineshape in the absence of the quadrupole interaction. Then Eq. (A9), in view of these approximations, becomes

$$G(\nu) = 0.4 G_0(\nu) + 0.6 \int_{-\infty}^{\infty} d(\Delta\nu) G_0(\nu + \Delta\nu) G_q(\Delta\nu). \quad (A10)$$

If  $G_0(\nu)$  is a gaussian with second moment  $\langle \Delta\nu^2 \rangle_0$  then

$$G(\nu) = 0.6 [2\pi(\langle \Delta\nu^2 \rangle_0 + \langle \Delta\nu^2 \rangle_q)]^{-\frac{1}{2}} \exp[-\nu^2/2(\langle \Delta\nu^2 \rangle_0 + \langle \Delta\nu^2 \rangle_q)] + \\ + 0.4 [2\pi\langle \Delta\nu^2 \rangle_0]^{-\frac{1}{2}} \exp[-\nu^2/2\langle \Delta\nu^2 \rangle_0], \quad (A11)$$

where  $\nu$  is centered at the Larmor frequency. Thus the second moment  $\langle \Delta\nu^2 \rangle$  of the composite line is

$$\langle \Delta\nu^2 \rangle = \langle \Delta\nu^2 \rangle_0 + 0.6 \langle \Delta\nu^2 \rangle_q. \quad (A12)$$

The Fourier transform of  $G(\nu)$  is the FID function. Thus the quadrupolar broadened FID should have the form of Eq. (19) with  $I_1/I_2 = 2/3$  and

$$\delta^2 = \alpha^2 + 4\pi^2 \langle \Delta\nu^2 \rangle_Q.$$

## REFERENCES

1. J. H. van Vleck, Phys. Rev. 74, 1168 (1948).
2. R. G. Shulman, B. J. Wyluda, and H. J. Hrostowski, Phys. Rev. 109, 808 (1958).
3. R. G. Shulman, J. M. Mays, and D. W. McCall, Phys. Rev. 100, 692 (1955).
4. M. A. Ruderman and C. Kittel, Phys. Rev. 96, 99 (1954).
5. N. Bloembergen and T. J. Rowland, Phys. Rev. 97, 1679 (1955).
6. P. W. Anderson, Phys. Rev. 99, 623 (1955).
7. R. K. Sundfors, Phys. Rev. 185, 458 (1969).
8. M. Engelsberg and R. E. Norberg, Phys. Rev. B 5, 3395 (1972).
9. E. H. Rhoderick, J. Phys. Chem. Solids 8, 498 (1958).
10. M. Cohen, Phil. Mag. 3, 565 (1958).
11. D. Gill and N. Bloembergen, Phys. Rev. 129, 2398 (1963).
12. H. R. Potts and G. L. Pearson, J. Appl. Phys. 37, 2098 (1966).
13. S. Clough and W. I. Goldburg, J. Chem. Phys. 45, 4080 (1966).
14. E. Brun, R. J. Mahler, H. Mahon, and W. L. Pierce, Phys. Rev. 129, 1965 (1963).
15. R. Kubo and T. Nagamiya, Solid State Physics, (McGraw-Hill, New York, 1969), p. 690.
16. H. Cramer, Mathematical Methods of Statistics, (Princeton Univ. Press, Princeton, N.J., 1946), Chapt. 17.

17. If the entire lattice sum is replaced by an integral  $\int_a^\infty \rho r^4 d^3r$ , where  $a$  is the minimum distance from the resonant nuclei to the impurity, then the second moment becomes

$$\langle \Delta H^2 \rangle_Q = \frac{24\pi}{5} [4I(I+1) - 3] \left( \frac{AR_{14}e^*}{\epsilon \chi_I \hbar} \right)^2 \left( \frac{\rho_I}{a} \right) f(\theta).$$

Thus  $a$  acts as a scaling parameter on the size of the quadrupole interaction.

One should be able to use the data to identify a preferred sublattice for the impurities. This result is qualitatively true, but the lattice sum is more accurate, and it, as well, reflects the location of the impurities through the quadrupolar second moment.

18. G. L. Pearson, H. R. Potts, V. G. Macres, Proceedings of the 7th International Conference on the Physics of Semiconductors, Damage in Semiconductors (Dunod Cie., Paris, 1965), p. 197.
19. D. L. Kendall, in Semiconductors and Semimetals, edited by R. K. Williardson and A. G. Beer (Academic Press, New York, 1968), Vol. 4, Chapt. 3.
20. J. D. Ellett, M. G. Gibby, U. Haeberlen, L. M. Huber, M. Mehring, A. Pines, and J. S. Waugh, Advances in Magnetic Resonance 5, 117 (1971).
21. I. J. Lowe and C. E. Tarr, J. Sci. Instrum. (Series 2) 1, 320 (1968).
22. I. J. Lowe and R. E. Norberg, Phys. Rev. 107, 46 (1957).
23. D. E. Barnaal and I. J. Lowe, Phys. Rev. Letters 11, 258 (1963).
24. P. R. Bevington, Data Reduction and Error Analysis for the Physical Sciences (McGraw-Hill Book Co., New York, 1969), Ch. 11.
25. A. Abragam, The Principles of Nuclear Magnetism (Oxford University Press, London, 1969), Ch. IV.

26. The fitting function

$$g(t) = I \exp[-\alpha^2 t^2 / 2(1 + \rho^2 t^2)^{1/2}] [0.4 + 0.6 \exp(-S^2 t^2 / 2)] \sin \beta t / \beta t$$

was used to approximate the effect of the like exchange interaction. The property of this function is that at small times it looks like Eq. (19), but at large times it looks exponential. The fourier transform, the cw absorption  $\chi''$ , has the character that near the center of the resonance it appears lorentzian and near the edge of the resonance line it appears gaussian. The ratio of fourth moment to second moment can be increased with the parameter  $\rho$ . This approximates the effect of the like spin exchange interaction. Unfortunately when this function was used our fitting routine failed to converge.

- 27. W. A. Harrison, Phys. Rev. B 8, 4487 (1973).
- 28. K. Yosida and T. Moriya, J. Phys. Soc. Japan 11, 33 (1956).
- 29. N. Bloembergen and P. P. Sorokin, Phys. Rev. 110, 865 (1958).
- 30. W. A. Harrison, private communication.
- 31. N. N. Sirota, in Semiconductors and Semimetals, edited by R. K. Willardson and A. G. Beer (Academic, New York, 1968), Vol. 4, Ch. 2.
- 32. An attempt was made to determine whether the defect density is dependent upon sample volume. Two samples were quenched from 600°C in tubes of different volumes, but no volume dependence was detected. However, subsequent analysis indicates some inaccuracy in the second moment measurements after a 600°C quench. Thus our observation of no volume dependence is not conclusive.

33. For comparison, we can examine Sundfors's theoretical model.<sup>7</sup> He sets  $\epsilon = 1$ ,  $e = e^*$ , and then computes  $\langle \Delta v^2 \rangle_\phi$  from Eq. (A3) by setting  $r$  equal to one-half the average distance between impurities,  $r = 1/2(3/4\pi\rho_I)^{1/3}$ , and averaging over  $\phi$ . This yields:

$$\langle \Delta v^2 \rangle_\phi = (4\pi\rho_I/3)^{4/3} e^4 Q^2 R_{14}^2 h^{-2} f(\theta).$$

Using his experimental values of  $\langle \Delta v^2 \rangle_\phi$  he calculated values of  $R_{14}$  that differ from other experimental values obtained by more direct means<sup>11</sup> by a factor of three. While Sundfors's expression for  $\langle \Delta v^2 \rangle_\phi$  has the correct angular dependence, it will not produce the correct numerical results.